MULTIPLE SCATTERING FROM N SPHERES USING MULTIPOLE REEXPANSION

NAIL A. GUMEROV AND RAMANI DURAISWAMI *

Abstract. A semi-analytical technique for the solution of problems of wave scattering from multiple spheres is developed. This technique extensively uses the theory for the translation and rotation of Helmholtz multipoles that was developed in our earlier work (Gumerov & Duraiswami, 2001). Results are verified by comparison with commercial boundary element software. The method developed is likely to be very useful in developing fast algorithms for many important problems, including those arising in simulations of composite media and multiphase flow.

Key words. multiple scattering, Helmholtz equation, spherical harmonics, Multipole expansions

1. Introduction. Numerous practical problems of acoustic and electromagnetic wave propagation require computation of the field scattered by multiple objects. Examples include scattering of acoustic waves by objects (e.g., the scattering of sound by humans and the environment), light scattering by clouds and environment, electromagnetic waves in composite materials and the human body, pressure waves in disperse systems (aerosols, emulsions, bubbly liquids), etc. Fast and reliable solution of forward scattering problems are especially required for solving inverse problems arising, for example, in medical tomography, mine detection, and radar. Our interest is in the modeling the cues that arise due to scattering of sound and light, and to use this information in simulating audio and video reality (Duraiswami et al, 2000).

In many cases the scatterers are spheres, or can be modeled as such. Such modeling is convenient for parametrization of large problems, since each sphere can be characterized by a few (say five) parameters, such as the three Cartesian coordinates of its center, its radius, and its impedance. This impedance will in general be a complex quantity, and characterizes the absorbing/reflecting properties of the body/surface. For example, we are exploring the modeling of the human head and body using two spheres representing respectively the head and the torso. In fluid mechanical problems, bubbles or dust particles can be assumed spherical (Gumerov et al (1988), Duraiswami and Prosperetti (1995)).

Starting with the multisphere representation, we can also deal with the effect of perfectly reflecting surfaces, such as walls in flow channels, room walls and the floor by replacing such surfaces with image spheres. For example, the acoustic field in a rectangular room with reflecting walls and a single scattering sphere inside can be modelled by a set of image sources and spheres (Duraiswami et al, 2001).

However, analytical solutions of the 3-D wave equation or the Helmholtz equation are available for only very limited configurations of sphere geometries and boundary conditions. Usually, such solutions are represented as infinite series of special functions (such as in the simplest case of a single sphere). In addition, only in the cases of a single sphere and two spheres is it possible to introduce separable systems of curvilinear coordinates for which the sphere surface(s) coincide with a coordinate surface, leading to simplified treatment of boundary conditions. These cases cannot cover the case of, say three or more spheres, but are useful as they provide an idea on the physics of scattering by spherical objects. In the general case one can expect only numerical, or approximate solutions.

Numerical methods for solution of the Helmholtz equation in arbitrary domains, such as boundary-element methods (BEM), finite-element methods (FEM), or finite difference methods (FDM), are well known and extensively used in research and commercial applications. Despite the relative advantages of these methods they all share a common deficiency related to the necessity of discretization of either the boundary surfaces, or of the complete space. Discretization introduces a characteristic size (or length scale) l_* of the surface or spatial element. For accurate and stable computations the change of discretization length l_* must not affect the results of computations of the scattered field. This leads to a requirement that this size theoretically should be much smaller than the wavelength λ, $l_* \ll \lambda$. Practically this condition is $l_* < B\lambda$,where B is some constant smaller than 1. If computations are required for high frequencies (or short waves), this condition of stability/accuracy leads to very fine surface or spatial meshes. For example, for 20 kHz sound in air in normal conditions the wavelength is 1.7 cm. To compute scattering of such sound by a typical human head of diameter $D = 17$ cm the length of one surface element should be "much smaller"

*Perceptual Interfaces and Reality Laboratory, Institute for Advanced Computer Studies, University of Maryland, College Park, MD 20742. Research supported by National Science Foundation grant ITR 0086075. This document is issued as University of Maryland Institute for Advanced Computer Studies Technical report UMIACS-TR-2001-72, and also as University of Maryland, Department of Computer Science Technical Report CS-TR-4294.

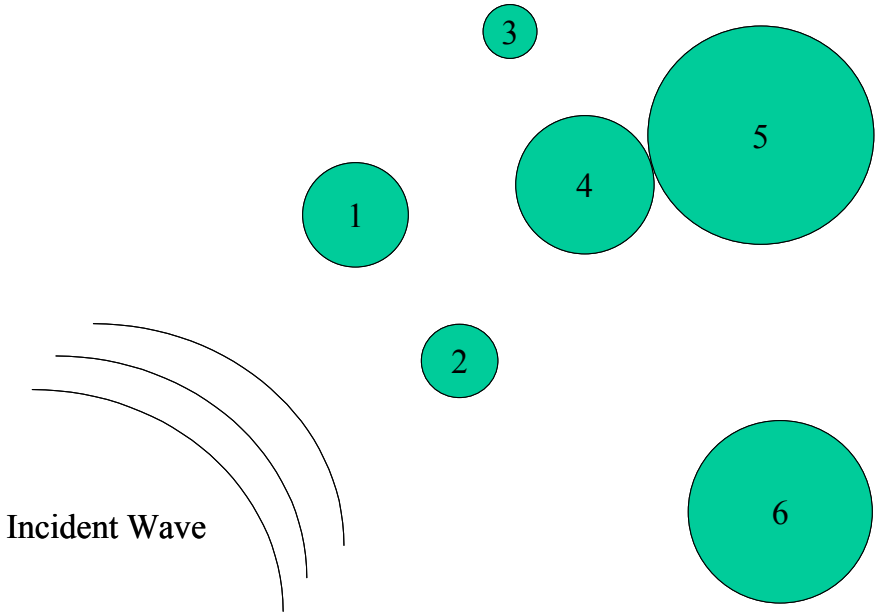

FIG. 2.1. *The multiple scattering problem considered in this paper.*

than 1.7 cm, say 6 times smaller than 1.7 cm, i.e. 60 times smaller than the diameter of the head. The total surface of the head is πD^2 and so the number of square elements should be of order $\pi \left(D/l_*\right)^2 \sim 12000$, this gives a 24000 element discretization of the head surface in case if triangular elements are used in BEM. Such discretization require inversion of large size element inter-influence matrices and are costly in terms of CPU time and memory, and cannot still be realized using even high end workstations.

For simplified geometries, such as multiple spheres, the scattering problem can be solved more efficiently using semi-analytical techniques. In the present report we develop such a method, which in some sense is analytical since it is based on solutions in the form of infinite series. At the same time the method is numerical, since in the simple form presented here, it requires inversion of a large size matrix for determining coefficients in the series, to satisfy boundary conditions on multiple spheres. The solution is based on decomposing the contributions of each scatterer to the total field, representation of each contribution in the form of series of spherical multipoles of the Helmholtz equation, and reexpansion of each multipole near the center of each sphere to satisfy boundary conditions. This procedure produces infinite linear systems in the coefficients of the expansions. This system can be solved numerically by truncation of the series.

We have developed software implementing this solution. We employ recently developed procedures of fast and stable computation of general multipole translation coefficients using recurrence relations (Gumerov & Duraiswami, 2001).[1] We compare results of computations with numerical and analytical solutions, and demonstrate the computational efficiency of our method with commercial BEM software. The results showed that the developed method compares favorably with commercial software in both accuracy and speed up of computations (in some cases by several orders of magnitude).

2. Statement of the Problem. Consider the problem of sound scattering by N spheres with radii $a_1, ..., a_N$ situated in an infinite 3 dimensional space as shown in Fig. 2.1. The coordinates of the center of each sphere are denoted as $\mathbf{r}'_p = (x'_p, y'_p, z'_p)$, $p = 1, ..., N$. The scattering problem in the frequency domain is reduced to solution of the Helmholtz equation for complex potential $\psi(\mathbf{r})$,

$$\nabla^2 \psi + k^2 \psi = 0, \tag{2.1}$$

[1] Since this reference will be repeated many times, in the sequel it will be written as (**GD2001**).

with the following impedance boundary conditions on the surface S_p of the pth sphere:

$$\left(\frac{\partial\psi}{\partial n}+i\sigma_p\psi\right)\Big|_{S_p}=0, \qquad p=1,...,N, \tag{2.2}$$

where k is the wavenumber and σ_j are constants characterizing impedance of each sphere, and $i=\sqrt{-1}$. In the particular case of sound-hard surfaces ($\sigma_p=0$) we have the Neumann boundary conditions,

$$\partial\psi/\partial n|_{S_p}=0, \tag{2.3}$$

and in the case of sound soft surfaces ($\sigma_p=\infty$) we have the Dirichlet boundary conditions,

$$\psi|_{S_p}=0. \tag{2.4}$$

Far from the region occupied by the spheres the complex potential tends to the potential of the incident wave $\psi_{in}(\mathbf{r})$:

$$\psi(\mathbf{r})|_{r\to\infty}\to\psi_{in}(\mathbf{r}). \tag{2.5}$$

Usually the potential is represented in the form:

$$\psi(\mathbf{r})=\psi_{in}(\mathbf{r})+\psi_{scat}(\mathbf{r}), \tag{2.6}$$

where $\psi_{scat}(\mathbf{r})$ is the potential of the scattered field. Far from the region occupied by spheres the scattered field should satisfy the Sommerfeld radiation condition:

$$\lim_{r\to\infty} r\left(\frac{\partial\psi_{scat}}{\partial r}-ik\psi_{scat}\right)=0. \tag{2.7}$$

3. Solution Using Multipole Translation Reexpansion.

3.1. Decomposition of the Scattered Field. Due to the linearity of the problem the scattered field can be represented in the form

$$\psi_{scat}(\mathbf{r})=\sum_{p=1}^{N}\psi_p(\mathbf{r}), \tag{3.1}$$

where $\psi_p(\mathbf{r})$ can be thought of as the field scattered by the pth sphere. Each potential $\psi_p(\mathbf{r})$ is a regular outside the pth sphere and satisfies the Sommerfeld radiation condition

$$\lim_{r\to\infty} r\left(\frac{\partial\psi_p}{\partial r}-ik\psi_p\right)=0, \qquad p=1,...,N. \tag{3.2}$$

3.2. Multipole Expansion. Let us introduce N reference frames connected with the center of each sphere. In spherical polar coordinates $\mathbf{r}-\mathbf{r}'_p=\mathbf{r}_p=(r_p,\theta_p,\varphi_p)$, solution of the Helmholtz equation that satisfy the radiation condition can be represented in the form

$$\psi_p(\mathbf{r})=\sum_{n=0}^{\infty}\sum_{m=-n}^{n}A_n^{(p)m}S_n^m(\mathbf{r}_p), \qquad p=1,...,N. \tag{3.3}$$

Here $A_n^{(p)m}$ are coefficients, $S_n^m(\mathbf{r})$ is a multipole of order n and degree m :

$$S_n^m(\mathbf{r}_p)=h_n(kr_p)Y_n^m(\theta_p,\varphi_p), \qquad p=1,...,N, \tag{3.4}$$

$h_n(kr)$ are spherical Hankel functions of the 1st kind that satisfy the Sommerfeld condition, and $Y_n^m(\theta,\phi)$ are orthonormal spherical harmonics, which also can be represented in the form

$$Y_n^m(\theta,\varphi)=(-1)^m\sqrt{\frac{2n+1}{4\pi}\frac{(n-|m|)!}{(n+|m|)!}}P_n^{|m|}(\cos\theta)e^{im\varphi}, \tag{3.5}$$
$$n=0,1,2,..., \qquad m=-n,...,n,$$

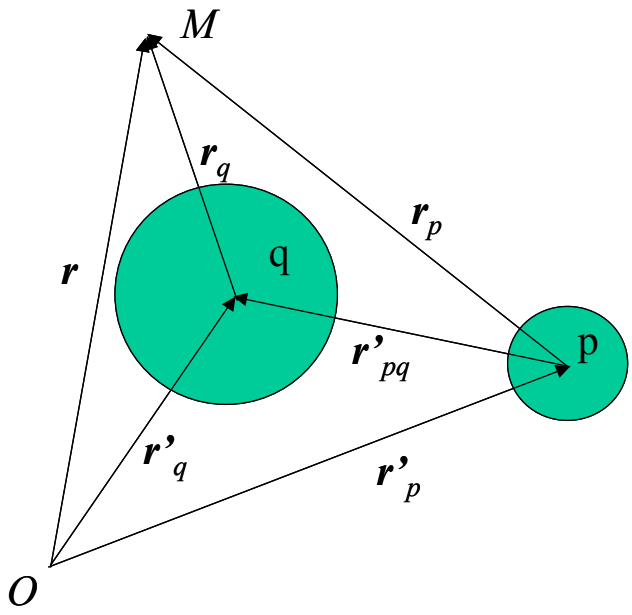

FIG. 3.1. *Notation denoting the different reference frames used in the multipole re-expansion technique.*

where $P_n^m(\mu)$ are the associated Legendre functions.

The problem now is to determine coefficients $A_n^{(p)m}$ so that *the complete potential*

$$\psi(\mathbf{r}) = \psi_{in}(\mathbf{r}) + \sum_{p=1}^{N}\sum_{n=0}^{\infty}\sum_{m=-n}^{n} A_n^{(p)m} S_n^m(\mathbf{r}_p) \tag{3.6}$$

satisfies all the boundary conditions on the surface of each sphere.

3.3. Multipole Reexpansion. To solve this problem let us consider the qth sphere. Near the center of this sphere, $\mathbf{r} = \mathbf{r}'_q$, all the potentials $\psi_p(\mathbf{r})$, are regular for $p \neq q$. Each multipole $S_n^m(\mathbf{r}_p), p \neq q$ can be then re-expanded into a series near this center, $|\mathbf{r}_q| \leqslant |\mathbf{r}'_p - \mathbf{r}'_q|$ as follows:

$$S_n^m(\mathbf{r}_p) = \sum_{l=0}^{\infty}\sum_{s=-l}^{l} (S|R)_{ln}^{sm}(\mathbf{r}'_{pq}) R_l^s(\mathbf{r}_q), \qquad p,q = 1,...,N, \qquad p \neq q. \tag{3.7}$$

Here $R_n^m(\mathbf{r}_q)$ are regular elementary solutions of the Helmholtz equation in spherical coordinates connected with the qth sphere:

$$R_n^m(\mathbf{r}_q) = j_n(kr_q)Y_n^m(\theta_q,\varphi_q), \qquad p = 1,...,N, \tag{3.8}$$

where $j_n(kr)$ are spherical Bessel functions of the first kind. The coefficients $(S|R)_{ln}^{sm}(\mathbf{r}'_{pq})$ are the translation reexpansion coefficients, and depend on the relative locations of the pth and qth spheres, $\mathbf{r}'_{pq}$. Since $\mathbf{r} = \mathbf{r}_p + \mathbf{r}'_p = \mathbf{r}_q + \mathbf{r}'_q$, we have

$$\mathbf{r}_p = \mathbf{r}_q + \mathbf{r}'_{pq}, \qquad \mathbf{r}'_{pq} = \mathbf{r}'_q - \mathbf{r}'_p = \mathbf{r}_p - \mathbf{r}_q, \tag{3.9}$$

where $\mathbf{r}'_{pq}$ is the vector directed from the center of the pth sphere to the center of the qth sphere. Detailed investigation of multipole reexpansion coefficients, their computation, their properties, and methods for efficient evaluation are considered in **GD2001**.

Near this center of expansion the incident field can be also represented using a similar series, the radius of convergence for which is not smaller than the radius of the qth sphere:

$$\psi_{in}(\mathbf{r}) = \sum_{l=0}^{\infty}\sum_{s=-l}^{l} C_l^{(in)s}(\mathbf{r}'_q) R_l^s(\mathbf{r}_q). \tag{3.10}$$

Substituting local expansions (3.7) and (3.10) into (3.6) we obtain the following representation of the field near $\mathbf{r} = \mathbf{r}'_q$

$$\psi(\mathbf{r}) = \sum_{l=0}^{\infty}\sum_{s=-l}^{l} C_l^{(in)s}\left(\mathbf{r}'_q\right) R_l^s(\mathbf{r}_q) + \sum_{n=0}^{\infty}\sum_{m=-n}^{n} A_n^{(q)m} S_n^m(\mathbf{r}_q) + \sum_{\substack{p=1\\p\neq q}}^{N}\sum_{n=0}^{\infty}\sum_{m=-n}^{n} A_n^{(p)m}\sum_{l=0}^{\infty}\sum_{s=-l}^{l}(S|R)_{ln}^{sm}\left(\mathbf{r}'_{pq}\right) R_l^s(\mathbf{r}_q).$$

Let us change the order of summation in the latter term and substitute expressions for S_n^m and R_n^m, (3.7) and (3.8). This expression then can be rewritten as

$$\psi(\mathbf{r}) = \sum_{l=0}^{\infty}\sum_{s=-l}^{l}\left[B_l^{(q)s} j_l(kr_q) + A_l^{(q)s} h_l(kr_q)\right] Y_l^s(\theta_q,\varphi_q), \tag{3.11}$$

$$B_l^{(q)s}(\mathbf{r}'_1,...,\mathbf{r}'_N) = C_l^{(in)s}\left(\mathbf{r}'_q\right) + \sum_{\substack{p=1\\p\neq q}}^{N}\sum_{n=0}^{\infty}\sum_{m=-n}^{n}(S|R)_{ln}^{sm}\left(\mathbf{r}'_{pq}\right) A_n^{(p)m}. \tag{3.12}$$

3.4. Boundary Conditions. From these equations we have the following relations for the boundary values of ψ and its normal derivative on the surface of the qth sphere

$$\psi|_{S_q} = \sum_{l=0}^{\infty}\sum_{s=-l}^{l}\left[B_l^{(q)s} j_l(ka_q) + A_l^{(q)s} h_l(ka_q)\right] Y_l^s(\theta_q,\varphi_q), \tag{3.13}$$

$$\left.\frac{\partial\psi}{\partial n}\right|_{S_q} = k\sum_{l=0}^{\infty}\sum_{s=-l}^{l}\left[B_l^{(q)s} j'_l(ka_q) + A_l^{(q)s} h'_l(ka_q)\right] Y_l^s(\theta_q,\varphi_q), \tag{3.14}$$

Satisfying boundary condition (2.2) on the surface of the qth sphere, we have

$$\sum_{l=0}^{\infty}\sum_{s=-l}^{l}\left\{B_l^{(q)s}\left[kj'_l(ka_q) + i\sigma_q j_l(ka_q)\right] + A_l^{(q)s}\left[kh'_l(ka_q) + i\sigma_q h_l(ka_q)\right]\right\} Y_l^s(\theta_q,\varphi_q) = 0. \tag{3.15}$$

Orthogonality of the surface harmonics yields:

$$B_l^{(q)s}\left[kj'_l(ka_q) + i\sigma_q j_l(ka_q)\right] + A_l^{(q)s}\left[kh'_l(ka_q) + i\sigma_q h_l(ka_q)\right] = 0, \qquad l = 0,1,..., \qquad s = -l,...,l. \tag{3.16}$$

Note that the boundary values of $\psi|_{S_q}$ and $\partial\psi/\partial n|_{S_q}$ can be expressed in terms of coefficients $A_l^{(q)s}$, since

$$B_l^{(q)s} = -A_l^{(q)s}\frac{kh'_l(ka_q) + i\sigma_q h_l(ka_q)}{kj'_l(ka_q) + i\sigma_q j_l(ka_q)}, \qquad l = 0,1,..., \qquad s = -l,...,l. \tag{3.17}$$

and formulae (3.13) and (3.14) yield

$$\psi|_{S_q} = \sum_{l=0}^{\infty}\sum_{s=-l}^{l}\left[h_l(ka_q) - j_l(ka_q)\frac{kh'_l(ka_q) + i\sigma_q h_l(ka_q)}{kj'_l(ka_q) + i\sigma_q j_l(ka_q)}\right] A_l^{(q)s} Y_l^s(\theta_q,\varphi_q), \tag{3.18}$$

$$\left.\frac{\partial\psi}{\partial n}\right|_{S_q} = k\sum_{l=0}^{\infty}\sum_{s=-l}^{l}\left[h'_l(ka_q) - j'_l(ka_q)\frac{kh'_l(ka_q) + i\sigma_q h_l(ka_q)}{kj'_l(ka_q) + i\sigma_q j_l(ka_q)}\right] A_l^{(q)s} Y_l^s(\theta_q,\varphi_q). \tag{3.19}$$

These relations can be also rewritten in a compact form using the Wronskian for the spherical Bessel functions,

$$W\{j_l(ka), h_l(ka)\} = j_l(ka)h'_l(ka) - j'_l(ka)h_l(ka) = i(ka)^{-2} \tag{3.20}$$

as

$$\psi|_{S_q} = \frac{1}{ika_q^2}\sum_{l=0}^{\infty}\sum_{s=-l}^{l}\frac{A_l^{(q)s}Y_l^s(\theta_q,\varphi_q)}{kj_l'(ka_q)+i\sigma_q j_l(ka_q)}, \tag{3.21}$$

$$\left.\frac{\partial\psi}{\partial n}\right|_{S_q} = -\frac{\sigma_q}{ka_q^2}\sum_{l=0}^{\infty}\sum_{s=-l}^{l}\frac{A_l^{(q)s}Y_l^s(\theta_q,\varphi_q)}{kj_l'(ka_q)+i\sigma_q j_l(ka_q)} = -i\sigma_q\,\psi|_{S_q}\,. \tag{3.22}$$

For the particular case of a sound-hard spheres ($\sigma_q = 0$) this gives

$$\psi|_{S_q} = \frac{1}{ik^2a_q^2}\sum_{l=0}^{\infty}\sum_{s=-l}^{l}\frac{A_l^{(q)s}Y_l^s(\theta_q,\varphi_q)}{j_l'(ka_q)}, \qquad \left.\frac{\partial\psi}{\partial n}\right|_{S_q} = 0, \tag{3.23}$$

while for sound-soft ($\sigma_q = \infty$) we have

$$\psi|_{S_q} = 0, \qquad \left.\frac{\partial\psi}{\partial n}\right|_{S_q} = \frac{i}{ka_q^2}\sum_{l=0}^{\infty}\sum_{s=-l}^{l}\frac{A_l^{(q)s}Y_l^s(\theta_q,\varphi_q)}{j_l(ka_q)}. \tag{3.24}$$

3.5. Matrix Representation. To determine the boundary values of the potential and/or its normal derivative and obtain a spatial distribution according (3.6) we need to determine the coefficients $A_l^{(q)s}$ in equations (3.16) and (3.12), which are valid for any sphere, $q = 1, ..., N$.

These equations form a linear system that may be represented in standard matrix-vector form. This can be accomplished in different ways according to the problem.

First, we note that coefficients of expansions to spherical harmonics, such as $A_n^m, n = 0, 1, 2, ...; m = -n, ..., n$, can be aligned into one column vector, e.g.

$$\mathbf{A} = \left(A_0^0, A_1^{-1}, A_1^0, A_1^1, A_2^{-2}, A_2^{-1}, A_2^0, A_2^1, A_2^2, ...\right)^T, \tag{3.25}$$

where the superscript T denotes the transpose. In this representation the elements of the vector $\mathbf{A}$ are related to coefficients A_n^m by

$$A_t = A_n^m, \qquad t = (n+1)^2 - (n-m), \quad n = 0, 1, 2, ...; \quad m = -n, ..., n; \quad t = 1, 2, ... \tag{3.26}$$

The same reduction in dimension can be applied to coefficients of reexpansion, $(S|R)_{ln}^{sm}$. Instead of a 4 dimensional matrix the coefficients can be packed in a 2 dimensional matrix as

$$(\mathbf{S}|\mathbf{R}) = \begin{pmatrix} (S|R)_{00}^{00} & (S|R)_{01}^{0-1} & (S|R)_{01}^{00} & (S|R)_{01}^{01} & (S|R)_{02}^{0-2} & ... \\ (S|R)_{10}^{-10} & (S|R)_{11}^{-1-1} & (S|R)_{11}^{-10} & (S|R)_{11}^{-11} & (S|R)_{12}^{-1-2} & ... \\ (S|R)_{10}^{00} & (S|R)_{11}^{0-1} & (S|R)_{11}^{00} & (S|R)_{11}^{01} & (S|R)_{12}^{0-2} & ... \\ (S|R)_{10}^{10} & (S|R)_{11}^{1-1} & (S|R)_{11}^{10} & (S|R)_{11}^{11} & (S|R)_{12}^{1-2} & ... \\ (S|R)_{20}^{-20} & (S|R)_{21}^{-2-1} & (S|R)_{21}^{-20} & (S|R)_{21}^{-21} & (S|R)_{22}^{-2-2} & ... \\ ... & ... & ... & ... & ... & ... \end{pmatrix}, \tag{3.27}$$

with the following correspondence of the matrix elements and coefficients:

$$\begin{aligned}(S|R)_{rt} = (S|R)_{ln}^{sm}, \qquad r = (l+1)^2 - (l-s), \quad t = (n+1)^2 - (n-m) \\ l, n = 0, 1, 2, ...; \quad m = -n, ..., n; \quad s = -l, ..., l.\end{aligned} \tag{3.28}$$

Using this representation we introduce the following vectors and matrices

$$\begin{aligned}\mathbf{A}^{(q)} = \left\{A_t^{(q)}\right\}^T, \quad \mathbf{D}^{(q)} = \left\{D_t^{(q)}\right\}^T, \quad \mathbf{L}^{(qp)} = \left\{L_{rt}^{(qp)}\right\}, \\ q = 1, ..., N, \quad p = 1, ..., N.\end{aligned} \tag{3.29}$$

where

$$
\begin{aligned}
A_t^{(q)} &= A_n^{(q)m}, \\
D_t^{(q)} &= -\frac{kj_n'(ka_q) + i\sigma_q j_n(ka_q)}{kh_n'(ka_q) + i\sigma_q h_n(ka_q)} C_n^{(in)m}\left(\mathbf{r}_q'\right), \\
L_{rt}^{(qp)} &= \frac{kj_l'(ka_q) + i\sigma_q j_l(ka_q)}{kh_l'(ka_q) + i\sigma_q h_l(ka_q)} (S|R)_{ln}^{sm}\left(\mathbf{r}_{pq}'\right), \quad \text{for } p \neq q, \\
L_{rt}^{(qq)} &= \delta_{rt}, \\
t &= (n+1)^2 - (n-m), \quad n = 0,1,2,...; \quad m = -n,...,n; \\
r &= (l+1)^2 - (l-s), \quad l = 0,1,2,...; \quad s = -l,...,l. \\
q &= 1,...,N, \quad p = 1,...,N,
\end{aligned}
\tag{3.30}
$$

where δ_{rt} is the Kronecker delta, $\delta_{rt} = 0$ for $r \neq t$ and $\delta_{rr} = 1$.

Equations (3.16) and (3.12) then can be represented in the form

$$
\sum_{p=1}^{N} \mathbf{L}^{(qp)} \mathbf{A}^{(p)} = \mathbf{D}^{(q)}, \quad q = 1,...,N. \tag{3.31}
$$

This system of equations can be represented as a single equation of the form

$$
\mathbf{LA} = \mathbf{D}, \tag{3.32}
$$

where the total matrices and vectors can be formed as

$$
\mathbf{L} = \begin{pmatrix} \mathbf{L}^{(11)} & \mathbf{L}^{(12)} & ... & \mathbf{L}^{(1N)} \\ \mathbf{L}^{(21)} & \mathbf{L}^{(22)} & ... & \mathbf{L}^{(2N)} \\ ... & ... & ... & ... \\ \mathbf{L}^{(N1)} & \mathbf{L}^{(N2)} & ... & \mathbf{L}^{(NN)} \end{pmatrix}, \qquad \mathbf{A} = \begin{pmatrix} \mathbf{A}^{(1)} \\ \mathbf{A}^{(2)} \\ ... \\ \mathbf{A}^{(N)} \end{pmatrix}, \qquad \mathbf{D} = \begin{pmatrix} \mathbf{D}^{(1)} \\ \mathbf{D}^{(2)} \\ ... \\ \mathbf{D}^{(N)} \end{pmatrix}. \tag{3.33}
$$

This linear system can be solved numerically using standard routines, such as LU-decomposition.

An important issue is the truncation of the infinite series and corresponding truncation of the associated matrices. A first solution is that we select a number M of modes to retain for each expansion. This number is selected via a heuristic based on the magnitude of the smallest retained term. In this case $n = 0,1,...,M$, $m = -n,...,n$, then the length of each vector $\mathbf{A}^{(p)}$ and $\mathbf{D}^{(p)}$ will be $(M+1)^2$, and the size of each sub-matrix $\mathbf{L}^{(qp)}$ will be $(M+1)^2 \times (M+1)^2$, the size of the total vectors $\mathbf{A}$ and $\mathbf{D}$ will be $N(M+1)^2$ and the size of the total matrix $\mathbf{L}$ will be $N(M+1)^2 \times N(M+1)^2$.

Several areas of research are ongoing to improve the solution procedure. We are currently investigating the use of fast multipole methods to solve these equations iteratively. Also, we are trying to put the heuristics used for truncation of the series on a more firm basis.

3.6. Computation of Multipole Reexpansion Coefficients. The $(S|R)$-multipole translation coefficients can be computed in different ways including via numerical evaluation of integral representations, or using the Clebsch-Gordan or 3-j Wigner symbols (e.g. see Epton & Dembart, 1994, Koc et al., 1999). For fast, stable, exact and efficient computations of the entire matrix of the reexpansion coefficients we used a method based on recurrence relations, which we have developed. We refer the reader to **GD2001** for proofs and details, and only provide necessary relations and initial values for using the recurrence procedures here.

All the $(S|R)_{ln}^{sm}\left(\mathbf{r}_{pq}'\right)$ translation reexpansion coefficients can be computed in the following way. First, we compute so-called "sectorial coefficients" of type $(S|R)_{l|m|}^{sm}$ and $(S|R)_{|s|n}^{sm}$ using the following relations:

$$
\begin{aligned}
b_{m+1}^{-m-1}(S|R)_{l,m+1}^{s,m+1} &= b_l^{-s}(S|R)_{l-1,m}^{s-1,m} - b_{l+1}^{s-1}(S|R)_{l+1,m}^{s-1,m}, \\
l &= 0,1,... \qquad s = -l,...,l, \qquad m = 0,1,2,....
\end{aligned}
\tag{3.34}
$$

$$
\begin{aligned}
b_{m+1}^{-m-1}(S|R)_{l,m+1}^{s,-m-1} &= b_l^{s}(S|R)_{l-1,m}^{s+1,-m} - b_{l+1}^{-s-1}(S|R)_{l+1,m}^{s+1,-m}, \\
l &= 0,1,... \qquad s = -l,...,l, \qquad m = 0,1,2,....
\end{aligned}
\tag{3.35}
$$

where

$$b_n^m = \begin{cases} \sqrt{\frac{(n-m-1)(n-m)}{(2n-1)(2n+1)}}, & 0 \leqslant m \leqslant n, \\ -\sqrt{\frac{(n-m-1)(n-m)}{(2n-1)(2n+1)}}, & -n \leqslant m < 0 \\ 0, & |m| > n, \end{cases}, \tag{3.36}$$

and the recurrence process starts with

$$(S|R)_{l0}^{s0}\left(\mathbf{r}'_{pq}\right) = \sqrt{(4\pi)}\,(-1)^l\, S_l^{-s}\left(\mathbf{r}'_{pq}\right), \quad (S|R)_{0n}^{0m}\left(\mathbf{r}'_{pq}\right) = \sqrt{(4\pi)} S_n^m\left(\mathbf{r}'_{pq}\right). \tag{3.37}$$

Due to the symmetry relation

$$(S|R)_{|m|l}^{-m,-s} = (-1)^{l+m}\,(S|R)_{l|m|}^{sm}, \tag{3.38}$$
$$l = 0, 1, 2, ..., \qquad s = -l, ..., l, \qquad m = -n, ..., n,$$

all of the sectorial coefficients $(S|R)_{|s|n}^{sm}$ can be obtained from the coefficients $(S|R)_{l|m|}^{sm}$.

Once the sectorial coefficients are computed all other coefficients can be derived from them using the following recurrence relation, which does not change the degrees s, m of the reexpansion coefficients:

$$a_{n-1}^m\,(S|R)_{l,n-1}^{sm} - a_n^m\,(S|R)_{l,n+1}^{sm} = a_l^s\,(S|R)_{l+1,n}^{sm} - a_{l-1}^s\,(S|R)_{l-1,n}^{sm}, \tag{3.39}$$
$$l, n = 0, 1, ... \qquad s = -l, ..., l, \qquad m = -n, ..., n,$$

where

$$a_n^m = \begin{cases} \sqrt{\frac{(n+1+|m|)(n+1-|m|)}{(2n+1)(2n+3)}}, & n \geqslant |m|, \\ 0, & |m| > n. \end{cases}. \tag{3.40}$$

Due to symmetry

$$(S|R)_{ln}^{sm} = (-1)^{n+l}\,(S|R)_{nl}^{-m,-s}, \tag{3.41}$$
$$l, n = 0, 1, ... \qquad s = -l, ..., l, \qquad m = -n, ..., n.$$

only those coefficients with $l \geqslant n$ need be computed using recurrence relations.

Also, the $(S|R)$ coefficients for any pair of spheres p an q need be computed only for the vector $\mathbf{r}'_{pq}$, since for the opposite directed vector we have:

$$(S|R)_{ln}^{sm}\left(\mathbf{r}'_{qp}\right) = (-1)^{l+n}\,(S|R)_{ln}^{sm}\left(\mathbf{r}'_{pq}\right), \quad l, n = 0, 1, ..., \quad m = -n, ..., n. \tag{3.42}$$

4. General Computational Algorithm. A flow chart of the computational algorithm is shown in Fig. 4.1.

Software based on this algorithm was developed and entitled MultisphereHelmholtz. Results of tests using this software are discussed below.

5. Coaxial Spheres. The case of two spheres is interesting, since on one hand the scattered fields due to the two spheres interact with each other (multiple scattering), while on the other the interaction is still simple enough that it can be investigated in more and understood more intuitively than the general case of N spheres. Additionally, in this case, the computation of the reexpansion matrices can be simplified by proper selection of the reference frames. Indeed, for two spheres we can introduce a reference frame which has its z axis directed from the center of one sphere to the center of the other sphere. Since the reexpansion coefficients depend only on the relative locations of the spheres, for this frame orientation, there will be no angular dependence of these coefficients. The same statement holds for the case when there are N spheres arranged along a line, taken to be the z axis. In these particular cases, the general reexpansion formula (3.7) simplifies to

$$S_n^m\left(\mathbf{r}_p\right) = \sum_{l=|m|}^{\infty} (S|R)_{ln}^{mm}\left(\mathbf{r}'_{pq}\right) R_l^m\left(\mathbf{r}_q\right), \qquad p = 1, ..., N, \qquad p \neq q. \tag{5.1}$$

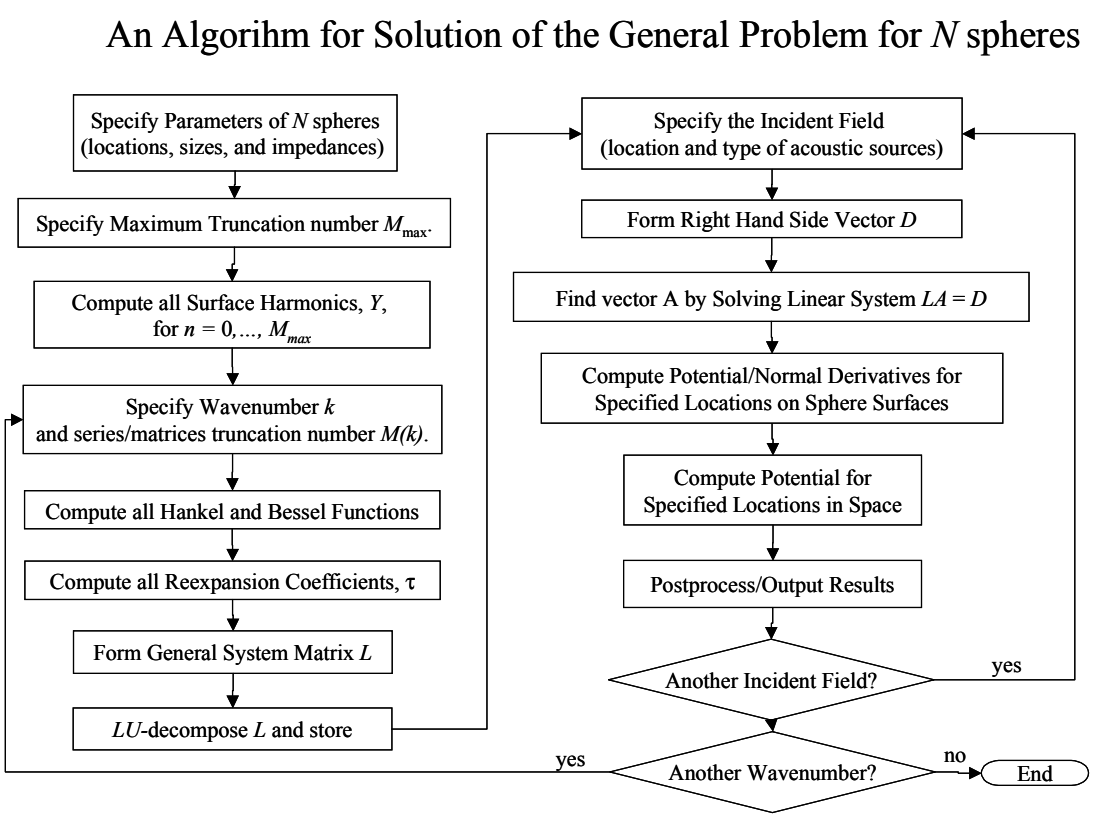

FIG. 4.1. *Flow chart of the general computational algorithm.*

The coefficients

$$(S|R)_{ln}^{m}\left(r'_{pq}\right)=(S|R)_{ln}^{mm}\left(\mathbf{r}'_{pq}\right),\quad l,n=0,1,...,\quad m=-n,...,n, \tag{5.2}$$

satisfy general recurrence relations and can be computed using the general algorithm we have developed. However, the simpler relations that take advantage of the co-axiality of the spheres result in faster computation, and provide substantially lower dimensional matrices. The recurrence relations and computational algorithm of the coaxial reexpansion coefficients can be found in our report (**GD2001**).

Note that the sign of coefficients $(S|R)_{ln}^{m}\left(r'_{pq}\right)$ depends on the direction of the vector $\mathbf{r}'_{pq}$. To be definite we select by convention that notation r'_{pq} corresponds to $\mathbf{r}'_{pq}$ and r'_{qp} corresponds to $\mathbf{r}'_{qp}=-\mathbf{r}'_{pq}$. Since $(S|R)_{ln}^{mm}\left(\mathbf{r}'_{pq}\right)=(-1)^{l+n}(S|R)_{ln}^{mm}\left(-\mathbf{r}'_{pq}\right)=(-1)^{l+n}(S|R)_{ln}^{mm}\left(\mathbf{r}'_{qp}\right)$ (see **GD2001**), we will have:

$$(S|R)_{ln}^{m}\left(r'_{pq}\right)=(-1)^{l+n}(S|R)_{ln}^{m}\left(r'_{qp}\right),\quad l,n=0,1,...,\quad m=-n,...,n. \tag{5.3}$$

5.1. Matrix Representation. According (5.1) harmonics of each degree m can be considered independently. Equations (3.12) and (3.16) can be rewritten in the form:

$$\frac{kj'_l(ka_q)+i\sigma_q j_l(ka_q)}{kh'_l(ka_q)+i\sigma_q h_l(ka_q)}\sum_{\substack{p=1\\p\neq q}}^{N}\sum_{n=|m|}^{\infty}(S|R)_{ln}^{m}\left(r'_{pq}\right)A_n^{(p)m}+A_l^{(q)m}=D_l^{(q)m}, \tag{5.4}$$

$$m=0,\pm1,\pm2,...,\quad l=|m|,|m|+1,...,\quad q=1,...,N,$$

where

$$D_l^{(q)m}=-\frac{kj'_l(ka_q)+i\sigma_q j_l(ka_q)}{kh'_l(ka_q)+i\sigma_q h_l(ka_q)}C_l^{(in)m}\left(\mathbf{r}'_q\right),\qquad m=0,\pm1,\pm2,...,\quad l=|m|,|m|+1,...,\quad q=1,...,N. \tag{5.5}$$

This linear system can be represented in the following form

$$\sum_{p=1}^{N} \mathbf{L}^{(qp)m} \mathbf{A}^{(p)m} = \mathbf{D}^{(q)m}, \quad m = 0, \pm 1, \pm 2, ..., \quad q = 1, ..., N, \tag{5.6}$$

where the vectors $\mathbf{A}^{(q)m}$ and $\mathbf{D}^{(q)m}$ and matrices $\mathbf{L}^{(qp)m}$ are packed as follows

$$\mathbf{A}^{(q)} = \left\{ A_n^{(q)m} \right\}^T, \quad \mathbf{D}^{(q)m} = \left\{ D_n^{(q)m} \right\}^T, \quad \mathbf{L}^{(qp)m} = \left\{ L_{ln}^{(qp)m} \right\}, \tag{5.7}$$
$$q = 1, ..., N, \quad p = 1, ..., N, \quad m = 0, \pm 1, \pm 2, ..., \quad l, n = |m|, |m| + 1, ...$$

with the individual matrix elements given by

$$L_{ln}^{(qp)m} = \frac{k j_l'(ka_q) + i\sigma_q j_l(ka_q)}{k h_l'(ka_q) + i\sigma_q h_l(ka_q)} (S|R)_{ln}^m \left(r'_{pq}\right), \quad \text{for } p \neq q, \tag{5.8}$$
$$L_{ln}^{(qq)m} = \delta_{ln}.$$

Since all equations can be considered separately for each m, the linear system (5.6) can be written as

$$\mathbf{L}^m \mathbf{A}^m = \mathbf{D}^m, \quad m = 0, \pm 1, \pm 2, ..., \tag{5.9}$$

where

$$\mathbf{L}^m = \begin{pmatrix} \mathbf{L}^{(11)m} & \mathbf{L}^{(12)m} & ... & \mathbf{L}^{(1N)m} \\ \mathbf{L}^{(21)m} & \mathbf{L}^{(22)m} & ... & \mathbf{L}^{(2N)m} \\ ... & ... & ... & ... \\ \mathbf{L}^{(N1)m} & \mathbf{L}^{(N2)m} & ... & \mathbf{L}^{(NN)m} \end{pmatrix}, \quad \mathbf{A}^m = \begin{pmatrix} \mathbf{A}^{(1)m} \\ \mathbf{A}^{(2)m} \\ ... \\ \mathbf{A}^{(N)m} \end{pmatrix}, \quad \mathbf{D}^m = \begin{pmatrix} \mathbf{D}^{(1)m} \\ \mathbf{D}^{(2)m} \\ ... \\ \mathbf{D}^{(N)m} \end{pmatrix}. \tag{5.10}$$

As in the general case considered above, the infinite series and matrices should be truncated for numerical computation. If we limit ourselves to the first M modes in each expansion of spherical harmonics, so that $m = 0, \pm 1, ..., \pm M$, $n = |m|, |m| + 1, ..., M$, then the length of each vector $\mathbf{A}^{(p)m}$ and $\mathbf{D}^{(p)m}$ is $M + 1 - |m|$, the dimensions of each matrix $\mathbf{L}^{(qp)m}$ is $(M + 1 - |m|) \times (M + 1 - |m|)$, the size of the total vectors $\mathbf{A}^m$ and $\mathbf{D}^m$ are $N(M + 1 - |m|)$ and the size of the total matrix $\mathbf{L}^m$ is $N(M + 1 - |m|) \times N(M + 1 - |m|)$. The problem then is reduced to solution of $2M + 1$ independent linear systems for each m. Note that the coaxial, or diagonal, translation coefficients $(S|R)_{ln}^m \left(r'_{pq}\right)$ are symmetrical with respect to the sign of the degree m, $(S|R)_{ln}^m \left(r'_{pq}\right) = (S|R)_{ln}^{-m} \left(r'_{pq}\right)$ (see **GD2001**). Therefore the matrices $\mathbf{L}^m$ are also symmetrical (see (5.8))

$$\mathbf{L}^m = \mathbf{L}^{-m}, \quad m = 0, 1, 2, ..., \tag{5.11}$$

and can be computed only for non-negative m. At the same time the right-hand side vector $\mathbf{D}^m$, generally speaking, does not coincide with $\mathbf{D}^{-m}$, so that the solution $\mathbf{A}^m$ can be different from $\mathbf{A}^{-m}$.

Let us compare the number of operations required for determination of all expansion coefficients $A_n^{(q)m}$, $m = 0, \pm 1, ..., , \pm M$, $n = |m|, |m| + 1, ..., M$, $q = 1, ..., N$, using the general algorithm and using the algorithm for coaxial spheres. Assuming that a standard solver requires CK^3 operations to solve a linear system with matrix $K \times K$, where C is some constant, we can find solution using general algorithm for

$$N_{operations}^{(general)} = CN^3 (M + 1)^6 \tag{5.12}$$

operations. Using the algorithm for coaxial spheres we will spend $CN^3 (M + 1 - |m|)^3$ operations to obtain $A_n^{(q)m}$ for each $m = 0, \pm 1, ..., , \pm M$. The total number of operations will be therefore

$$N_{operations}^{(coaxial)} = CN^3 \sum_{m=-M}^{M} (M + 1 - |m|)^3 = CN^3 \left[(M + 1)^3 + 2 \sum_{m=1}^{M} m^3 \right] \tag{5.13}$$
$$= CN^3 \left[(M + 1)^3 + \frac{1}{2} M^2 (M + 1)^2 \right] = \frac{1}{2} CN^3 \left[(M + 1)^4 + (M + 1)^2 \right].$$

Therefore, for $M \gg 1$, we have

$$\frac{N_{operations}^{(general)}}{N_{operations}^{(coaxial)}} \sim 2M^2. \tag{5.14}$$

which shows much higher efficiency of the algorithm for coaxial spheres.

Note also that in the case of coaxial spheres the number of the multipole reexpansion coefficients that need to be computed for each pair $p \neq q$ requires $O(M^3)$ operations, while in general case such computations can be performed in $O(M^4)$ operations (see **GD2001**). These numbers are smaller than the leading order term in the complexity, that required for solution of linear equations, and thus evaluations (5.12)-(5.14) provide a comparison between two methods.

5.2. Rotation of the Reference Frame. The above expressions for coaxial spheres assume that the z axis coincides with the direction from the center of one of the spheres to the center of some other sphere. If coordinates of spheres are specified in original reference frame, with axis z oriented arbitrarily with respect to the line connected the sphere centers we can rotate them so that the new reference frame is convenient for use with the coaxial algorithm. Therefore we consider two reference frames: the original reference frame and the reference frame which axis z is directed say from sphere 1 to sphere 2. Denote the coordinates of an arbitrary point in the original reference frame as (x, y, z) and the coordinates of the same point in the rotated reference frame, with the same origin, as $(\widehat{x}, \widehat{y}, \widehat{z})$. Denote the unit coordinate vectors of the original coordinates as $(\mathbf{i}_x, \mathbf{i}_x, \mathbf{i}_z)$ and the unit vectors of the rotated reference frame as $(\mathbf{i}_{\widehat{x}}, \mathbf{i}_{\widehat{y}}, \mathbf{i}_{\widehat{z}})$. By definition, we have the following representations for an arbitrary vector $\mathbf{r}$:

$$\mathbf{r} = x\mathbf{i}_x + y\mathbf{i}_y + z\mathbf{i}_z = \widehat{x}\mathbf{i}_{\widehat{x}} + \widehat{y}\mathbf{i}_{\widehat{y}} + \widehat{z}\mathbf{i}_{\widehat{z}}. \tag{5.15}$$

Coordinates (x, y, z) and $(\widehat{x}, \widehat{y}, \widehat{z})$ are connected with the rotation matrix Q :

$$\begin{pmatrix} \widehat{x} \\ \widehat{y} \\ \widehat{z} \end{pmatrix} = Q \begin{pmatrix} x \\ y \\ z \end{pmatrix}, \quad \begin{pmatrix} x \\ y \\ z \end{pmatrix} = Q^* \begin{pmatrix} \widehat{x} \\ \widehat{y} \\ \widehat{z} \end{pmatrix}, \tag{5.16}$$

where

$$Q = \begin{pmatrix} \mathbf{i}_{\widehat{x}} \cdot \mathbf{i}_x & \mathbf{i}_{\widehat{x}} \cdot \mathbf{i}_y & \mathbf{i}_{\widehat{x}} \cdot \mathbf{i}_z \\ \mathbf{i}_{\widehat{y}} \cdot \mathbf{i}_x & \mathbf{i}_{\widehat{y}} \cdot \mathbf{i}_y & \mathbf{i}_{\widehat{y}} \cdot \mathbf{i}_z \\ \mathbf{i}_{\widehat{z}} \cdot \mathbf{i}_x & \mathbf{i}_{\widehat{z}} \cdot \mathbf{i}_y & \mathbf{i}_{\widehat{z}} \cdot \mathbf{i}_z \end{pmatrix}, \quad Q^* = Q^{-1} = \begin{pmatrix} \mathbf{i}_{\widehat{x}} \cdot \mathbf{i}_x & \mathbf{i}_{\widehat{y}} \cdot \mathbf{i}_x & \mathbf{i}_{\widehat{z}} \cdot \mathbf{i}_x \\ \mathbf{i}_{\widehat{x}} \cdot \mathbf{i}_y & \mathbf{i}_{\widehat{y}} \cdot \mathbf{i}_y & \mathbf{i}_{\widehat{z}} \cdot \mathbf{i}_y \\ \mathbf{i}_{\widehat{x}} \cdot \mathbf{i}_z & \mathbf{i}_{\widehat{y}} \cdot \mathbf{i}_z & \mathbf{i}_{\widehat{z}} \cdot \mathbf{i}_z \end{pmatrix}. \tag{5.17}$$

By definition

$$\mathbf{i}_{\widehat{z}} = \frac{\mathbf{r}_{12}}{|\mathbf{r}_{12}|} = \frac{\mathbf{r}_{12}}{r_{12}} = e_x\mathbf{i}_x + e_y\mathbf{i}_y + e_z\mathbf{i}_z, \quad e_x^2 + e_y^2 + e_z^2 = 1, \tag{5.18}$$

where e_x, e_y, and e_z are the direction cosines of $\mathbf{i}_{\widehat{z}}$, and

$$e_x = \frac{\mathbf{r}_{12} \cdot \mathbf{i}_x}{r_{12}}, \quad e_y = \frac{\mathbf{r}_{12} \cdot \mathbf{i}_y}{r_{12}}, \quad e_z = \frac{\mathbf{r}_{12} \cdot \mathbf{i}_z}{r_{12}}. \tag{5.19}$$

As it is shown in our previous report (**GD2001**) in this case the rotation matrix can be computed as a composition of two rotations:

$$Q = \begin{pmatrix} \cos\phi & -\sin\phi & 0 \\ \sin\phi & \cos\phi & 0 \\ 0 & 0 & 1 \end{pmatrix} \begin{pmatrix} -\frac{e_y}{\sqrt{(e_x^2+e_y^2)}} & \frac{e_x}{\sqrt{(e_x^2+e_y^2)}} & 0 \\ -\frac{e_z e_x}{\sqrt{(e_x^2+e_y^2)}} & -\frac{e_z e_y}{\sqrt{(e_x^2+e_y^2)}} & \sqrt{(e_x^2+e_y^2)} \\ e_x & e_y & e_z \end{pmatrix}, \tag{5.20}$$

where ϕ is an arbitrary angle, meaning that any rotation around the $\mathbf{i}_{\widehat{z}}$ preserves $\mathbf{i}_{\widehat{z}}$ and satisfies our requirement for a convenient reference frame. Particularly, for $\phi = 0$, the first multiplier in the right hand side of (5.20) is the identity matrix.

Obviously all relations for coaxial spheres and expansion coefficients $A_n^{(p)m}$ should be then treated in the rotated reference frame, which formally means addition of hats over all coordinates in the expressions derived. All spherical harmonics and multipoles represent solutions in the rotated reference frame and the incident field expansion coefficients $C_l^{(in)m}$ should also be found in the $(\mathbf{i}_{\widehat{x}}, \mathbf{i}_{\widehat{y}}, \mathbf{i}_{\widehat{z}})$ system of coordinates.

5.3. Computation of Coaxial Reexpansion Coefficients. Due to the symmetry relations (see (3.42) and (5.2)) and

$$(S|R)_{ln}^{m} = (S|R)_{ln}^{-m}, \qquad m = 0, 1, 2, ... \tag{5.21}$$

the coaxial coefficients $(S|R)_{ln}^{m}\left(\mathbf{r}'_{pq}\right)$ can be computed only for $l \geqslant n \geqslant m \geqslant 0$. The process of filling of the matrix $\{(S|R)_{ln}^{m}\}$ can be performed efficiently using recurrence relations that first fill the layers with respect to the orders l and n followed by advancement with respect to the degree m. If such a filling procedure is selected then the first step is filling of the layer $m = 0$. The initial value depends on the orientation of $\mathbf{r}'_{pq}$ vector relative to the axis $\mathbf{i}_z$ (or $\mathbf{i}_{\hat{z}}$ if rotation is performed), and is given by

$$(S|R)_{l0}^{0}\left(r'_{pq}\right) = (S|R)_{l0}^{00}\left(\mathbf{r}'_{pq}\right) = \sqrt{(4\pi)}(-1)^{l} S_{l}^{0}\left(\mathbf{r}'_{pq}\right) = \sqrt{(2l+1)} h_l(kr'_{pq}), \tag{5.22}$$

where

$$\epsilon_{lpq} = \left(-\frac{\mathbf{r}'_{pq}\cdot\mathbf{i}_z}{\left|\mathbf{r}'_{pq}\right|}\right)^{l} = \begin{cases} (-1)^l, & \text{for } \mathbf{r}'_{pq}\cdot\mathbf{i}_z = \left|\mathbf{r}'_{pq}\right| \\ 1, & \text{for } \mathbf{r}'_{pq}\cdot\mathbf{i}_z = -\left|\mathbf{r}'_{pq}\right| \end{cases}. \tag{5.23}$$

For advancement with respect to m it is convenient to use (5.4) for $n = m$,

$$b_{m+1}^{-m-1}\,(S|R)_{l,m+1}^{m+1} = b_{l}^{-m-1}\,(S|R)_{l-1,m}^{m} - b_{l+1}^{m}\,(S|R)_{l+1,m}^{m}, \quad l = m+1, m+2, ..., \tag{5.24}$$

with b's given by (3.36) and obtain other $(S|R)_{ln}^{m+1}$ using (3.39).

For the case the axis is directed in the opposite direction, the coefficients will have alternating signs. This is easy to establish using the definition (5.2) and the symmetries (3.42), (5.3), and (5.21).

5.4. Computational Algorithm. The computational algorithm for the case of coaxial spheres almost repeats the general algorithm. Peculiarities include rotation of the reference frame and the packing of the system matrix to reduce the memory complexity. Note that since computations are performed in the reference frame $(\mathbf{i}_{\hat{x}}, \mathbf{i}_{\hat{y}}, \mathbf{i}_{\hat{z}})$, all vectors and surface harmonics are represented in that frame. With respect to the computational reference frame, vectors such as $\mathbf{r}$ should be treated by applying the rotation matrix Q to them. To store the matrix (and its LU-decomposition) in an optimal way we use a multi-index packing in a one-dimensional array. The algorithm was realized in software entitled MultisphereHelmholtzCoaxial. The code was validated by comparisons with the general code MultisphereHelmholtz. Since both codes produced the same results in the case of coaxial spheres, no more discussions on comparisons of the results will provided in this report. As expected MultisphereHelmholtzCoaxial showed better performance compared to MultisphereHelmholtz to achieve the same accuracy (the same truncation number) in terms of CPU time and memory.

6. Typical Incident Fields. Below we consider explicit expressions for multipole expansion coefficients $C_{l}^{(in)s}\left(\mathbf{r}'_{q}\right)$ (see (3.10)) for several typical incident fields encountered in practical problems.

6.1. Monopole Source. In the case of a monopole source located at $\mathbf{r} = \mathbf{r}_{source}$, the incident field corresponds to the fundamental solution of the Helmholtz equation

$$\psi_{in}\left(\mathbf{r}\right) = QG_k\left(\mathbf{r} - \mathbf{r}_{source}\right) = Q\frac{e^{ik|\mathbf{r}-\mathbf{r}_{source}|}}{4\pi\left|\mathbf{r} - \mathbf{r}_{source}\right|}, \tag{6.1}$$

where Q is the source intensity (complex, if the phase Φ is not zero)

$$Q = |Q|\, e^{i\Phi}. \tag{6.2}$$

Expansion of this function near the center of the qth sphere $\mathbf{r} = \mathbf{r}'_q$ (see also Fig. 2) can be found elsewhere (e.g., Morse & Feshbach, 1953)

$$\psi_{in}\left(\mathbf{r}\right) = Qik\sum_{n=0}^{\infty}\sum_{m=-n}^{n} S_{n}^{-m}\left(\mathbf{r}_{source} - \mathbf{r}'_q\right) R_{n}^{m}\left(\mathbf{r}_q\right), \qquad |\mathbf{r}_q| \leqslant \left|\mathbf{r}_{source} - \mathbf{r}'_q\right|. \tag{6.3}$$

Comparing (3.10) and (6.3) we obtain

$$C_{n}^{(in)m}\left(\mathbf{r}'_q\right) = QikS_{n}^{-m}\left(\mathbf{r}_{source} - \mathbf{r}'_q\right). \tag{6.4}$$

6.2. Multiple Monopole Sources. This type of incident field is encountered not only when the field is generated by several real sources, but also when additional sources appear as images, as when planes of symmetry bound the domain. For example if we have a single sphere near an infinite rigid wall, and where the incident field is generated by a single monopole source, the problem in the half-space is equivalent to the problem in the whole space, but for two spheres and two sources. The image sphere and source are symmetrical to the real sphere and source with respect to this plane.

More generally, the incident field generated by N_s sources is

$$\psi_{in}\left(\mathbf{r}\right)=\sum_{\alpha=1}^{N_s}Q_\alpha G_k\left(\mathbf{r}-\mathbf{r}_\alpha^{(s)}\right), \tag{6.5}$$

where Q_α and $\mathbf{r}_\alpha^{(s)}$ are respectively the complex intensities and location of the αth source ($\alpha=1,...,N_s$). Using the expansion for a single source (6.3) near the center of the qth sphere $\mathbf{r}=\mathbf{r}_q'$, and superposing the field due to all sources, we have

$$\psi_{in}\left(\mathbf{r}\right)=ik\sum_{n=0}^{\infty}\sum_{m=-n}^{n}\sum_{\alpha=1}^{N_s}Q_\alpha S_n^{-m}\left(\mathbf{r}_\alpha^{(s)}-\mathbf{r}_q'\right)R_n^m\left(\mathbf{r}_q\right),\qquad \left|\mathbf{r}_q\right|\leqslant\left|\mathbf{r}_\alpha^{(s)}-\mathbf{r}_q'\right|. \tag{6.6}$$

Comparing (3.10) and (6.3) we obtain

$$C_n^{(in)m}\left(\mathbf{r}_q'\right)=ik\sum_{\alpha=1}^{N_s}Q_\alpha S_n^{-m}\left(\mathbf{r}_\alpha^{(s)}-\mathbf{r}_q'\right). \tag{6.7}$$

6.3. Plane Wave. The case of sound scattering by a rigid sphere placed in a plane wave was considered by Lord Rayleigh in the 19th century (Strutt, 1904, 1945). We include this case for generality and to provide some formulae for arbitrary locations of the origin of the reference frame. The incident field of the plane wave is described by

$$\psi_{in}\left(\mathbf{r}\right)=Qe^{i\mathbf{k}\cdot\mathbf{r}}, \tag{6.8}$$

where

$$\mathbf{k}=\left(k_x,k_y,k_z\right),\quad k_x^2+k_y^2+k_z^2=k^2, \tag{6.9}$$

is the wave vector, and Q is the complex amplitude of the wave (6.2).

Expansion of the field in spherical harmonics near the center of the qth sphere $\mathbf{r}=\mathbf{r}_q'$ can be obtained from the solution for monopole source, Equations (6.1) and (6.3), where we use an asymptotic expansion of the spherical Hankel function at large distances between the source and the sphere:

$$\psi_{in}\left(\mathbf{r}\right)=4\pi Q\left[r_{source}\frac{e^{ik\left|\mathbf{r}-\mathbf{r}_{source}\right|}}{4\pi\left|\mathbf{r}-\mathbf{r}_{source}\right|}\right]_{r_{source}\longrightarrow\infty}=4\pi Q\left[r_{source}ik\sum_{n=0}^{\infty}\sum_{m=-n}^{n}S_n^{-m}\left(\mathbf{r}_{source}-\mathbf{r}_q'\right)R_n^m\left(\mathbf{r}_q\right)\right]_{r_{source}\longrightarrow\infty} \tag{6.10}$$

$$=4\pi Q\left[ikr_{source}\sum_{n=0}^{\infty}\sum_{m=-n}^{n}h_n\left(kr_{q,source}\right)Y_n^{-m}(\theta_{q,source},\varphi_{q,source})R_n^m\left(\mathbf{r}_q\right)\right]_{r_{source}\longrightarrow\infty}$$

$$=4\pi Qe^{ikr_{q,source}}\sum_{n=0}^{\infty}\sum_{m=-n}^{n}i^{-n}Y_n^{-m}(\theta_{q,source},\varphi_{q,source})R_n^m\left(\mathbf{r}_q\right)$$

$$=4\pi Qe^{ikr_{q,source}}\sum_{n=0}^{\infty}\sum_{m=-n}^{n}(-1)^n i^{-n}Y_n^{-m}(\theta_k,\varphi_k)R_n^m\left(\mathbf{r}_q\right).$$

Here $\mathbf{r}_{q,source}=\mathbf{r}_{source}-\mathbf{r}_q'$, and the angles $\theta_k=\pi-\theta_{q,source}'$ and $\varphi_k=\pi+\varphi_{q,source}'$ determine the direction of the wave from the infinitely located source, and therefore they can be obtained from the known wave

vector (6.9) as

$$\begin{aligned} \sin\theta_k \cos\varphi_k &= k_x/k, \\ \sin\theta_k \sin\varphi_k &= k_y/k, \\ \cos\theta_k &= k_z/k. \end{aligned} \tag{6.11}$$

Now we note that $\mathbf{r} = \mathbf{r}'_q + \mathbf{r}_q$ (see Fig. 2). If we put $\mathbf{r}_q = \mathbf{0}$ in (6.10) and use $R_l^s(\mathbf{0}) = \sqrt{\frac{1}{4\pi}}\delta_{l0}\delta_{s0}$, we find that

$$\psi_{in}\left(\mathbf{r}'_q\right) = Qe^{ikr_{q,source}}, \tag{6.12}$$

and, more generally,

$$\psi_{in}(\mathbf{r}) = 4\pi\psi_{in}\left(\mathbf{r}'_q\right)\sum_{n=0}^{\infty}\sum_{m=-n}^{n}(-1)^n i^{-n}Y_n^{-m}(\theta_k,\varphi_k)R_n^m(\mathbf{r}_q). \tag{6.13}$$

On the other hand, using definition (6.8)

$$\psi_{in}\left(\mathbf{r}'_q\right) = Qe^{i\mathbf{k}\cdot\mathbf{r}'_q}. \tag{6.14}$$

Comparing (3.10) with (6.13) and (6.14), we obtain the following expression for $C_n^{(in)m}(\mathbf{r}'_1)$ as

$$C_n^{(in)m}\left(\mathbf{r}'_q\right) = 4\pi Qe^{i\mathbf{k}\cdot\mathbf{r}'_q}(-1)^n i^{-n}Y_n^{-m}(\theta_k,\varphi_k). \tag{6.15}$$

This result can be easily generalized to the case where the incident field is obtained from the superposition of N_w plane waves:

$$\psi_{in}(\mathbf{r}) = \sum_{\alpha=1}^{N_w} Q_\alpha e^{i\mathbf{k}_\alpha\cdot\mathbf{r}}, \qquad \mathbf{k}_\alpha = (k_{\alpha,x}, k_{\alpha,y}, k_{\alpha,z}), \quad k_{\alpha,x}^2 + k_{\alpha,y}^2 + k_{\alpha,z}^2 = k^2. \tag{6.16}$$

with intensities Q_α and incident angles $\theta_k^{(\alpha)}, \varphi_k^{(\alpha)}$, corresponding to the wave vectors $\mathbf{k}_\alpha$ ($\alpha = 1, ..., N_w$, see (6.11)). In this case we have

$$C_n^{(in)m}\left(\mathbf{r}'_q\right) = 4\pi(-1)^n i^{-n}\sum_{\alpha=1}^{N_w} Q_\alpha e^{i\mathbf{k}_\alpha\cdot\mathbf{r}'_\mathbf{q}}Y_n^{-m}(\theta_k^{(\alpha)},\varphi_k^{(\alpha)}). \tag{6.17}$$

6.4. Multipole Sources. The case of multipole sources is a practical one to consider, since real sources of sound (loudspeakers, turbulent vortices, etc.) usually have not only monopole, but also dipole, and quadrupole components. More generally, for the case of a multipole source of order n and degree m we have

$$\psi_{in}(\mathbf{r}) = QS_n^m(\mathbf{r} - \mathbf{r}_{source}), \tag{6.18}$$

where $\mathbf{r}_{source}$ is the location of the source, and Q is its complex amplitude. In this case, for determination of the expansion of the incident field near the center of the qth sphere we can use results obtained for multipole reexpansion (3.7)

$$S_n^m(\mathbf{r} - \mathbf{r}_{source}) = \sum_{l=0}^{\infty}\sum_{s=-l}^{l}(S|R)_{ln}^{sm}\left(\mathbf{r}'_q - \mathbf{r}_{source}\right)R_l^s(\mathbf{r}_q). \tag{6.19}$$

Coefficients $C_l^{(in)s}\left(\mathbf{r}'_q\right)$ then simply become

$$C_l^{(in)s}\left(\mathbf{r}'_q\right) = Q(S|R)_{ln}^{sm}\left(\mathbf{r}'_q - \mathbf{r}_{source}\right). \tag{6.20}$$

This result can be generalized to the incident field generated by N_s multipole sources, where each source has its own intensity Q_α, location $\mathbf{r}_\alpha^{(s)}$, order n_α, and degree m_α ($\alpha = 1, ..., N_s$) as

$$\psi_{in}(\mathbf{r}) = \sum_{\alpha=1}^{N_s} Q_\alpha S_{n_\alpha}^{m_\alpha}\left(\mathbf{r} - \mathbf{r}_\alpha^{(s)}\right), \tag{6.21}$$

For such a field, the coefficients $C_l^{(in)s}\left(\mathbf{r}'_q\right)$ can be computed as follows

$$C_l^{(in)s}\left(\mathbf{r}'_q\right) = \sum_{\alpha=1}^{N_s} Q_\alpha (S|R)_{ln_\alpha}^{sm_\alpha}\left(\mathbf{r}'_q - \mathbf{r}_\alpha^{(s)}\right). \tag{6.22}$$

Note that this formula covers many practical cases, where the field is generated by different types of sources and their images due to the presence of planes or other reflecting surfaces, if a representation of the type (6.21) is available for the particular geometry of the problem.

7. Example Problems. We apply our method to several example problems. First, we compare the semi-analytical solution we obtain with the purely numerical solutions obtained with the aid of the boundary element method (BEM) to determine the accuracy of solution, and identify problems that will be addressed in subsequent studies.

7.1. Single Sphere. For the case of single sphere there is no need to solve a linear system to account for the influence of neighboring spheres. However, this case is important from a practical point of view. We include this case for demonstration of the solution, comparison with the BEM, error evaluations, and to provide analytical solution for the problem of the field generated by an arbitrary multipole in the presence of a sphere.

In the case of single sphere ($N = 1, q = 1$) from (3.30) - (3.33) we have $\mathbf{L}^{(1)} = \mathbf{I}, \mathbf{A}^{(1)} = \mathbf{D}^{(1)}$, or

$$A_n^{(1)m} = -\frac{kj'_n(ka) + i\sigma j_n(ka)}{kh'_n(ka) + i\sigma h_n(ka)} C_n^{(in)m}\left(\mathbf{r}'_1\right), \tag{7.1}$$

Here and below in the case of a single sphere we will drop subscript 1 for σ and a, while keeping them for the coordinates. Substituting this expression into (3.21) and (3.22), we obtain expressions for the potential and its normal derivative on the sphere surface as

$$\psi|_{S_1} = -\frac{1}{ika^2}\sum_{l=0}^{\infty}\sum_{s=-l}^{l}\frac{C_l^{(in)s}\left(\mathbf{r}'_1\right) Y_l^s(\theta_1, \varphi_1)}{kh'_l(ka) + i\sigma h_l(ka)}, \tag{7.2}$$

$$\left.\frac{\partial\psi}{\partial n}\right|_{S_1} = \frac{\sigma}{ka^2}\sum_{l=0}^{\infty}\sum_{s=-l}^{l}\frac{C_l^{(in)s}\left(\mathbf{r}'_1\right) Y_l^s(\theta_1, \varphi_1)}{kh'_l(ka) + i\sigma h_l(ka)} = -i\sigma\ \psi|_{S_1}. \tag{7.3}$$

The coefficients $C_n^{(in)m}\left(\mathbf{r}'_1\right)$ are determined using (3.10) and depend on the incident field. We consider the following particular cases for the incident field.

7.1.1. Monopole Source. A simplification of general formula for $C_n^{(in)m}$ (6.4) is possible, since the problem for monopole source and a single sphere is axisymmetric relative to the axis connecting the center of the sphere and the location of the source. In this case selecting the axis z_1 to be the axis of symmetry, we have

$$C_n^{(in)m} = Qik\delta_{m0} h_n\left(k\left|\mathbf{r}_{source} - \mathbf{r}'_1\right|\right) Y_n^0(0,0) = Qik\delta_{m0}\sqrt{\frac{2n+1}{4\pi}} h_n(kd) = Qik\delta_{m0}\sqrt{\frac{2n+1}{4\pi}} h_n(kd), \tag{7.4}$$

where d is the distance between the source and the center of the sphere. In this most simplified case of the reference frame selection, expressions for the surface values of the potential and its derivative (7.2) and (7.3)

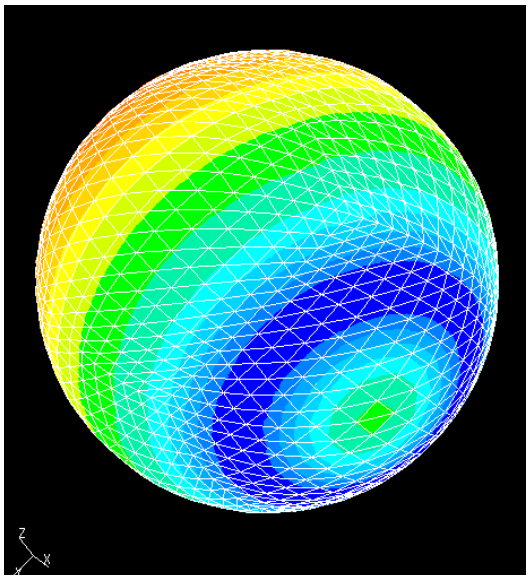

FIG. 7.1. *Typical computational mesh and output for the potential on the sphere surface using the BEM (Comet 4.0, Collins & Aikman Automotive Interior Systems).*

become

$$\psi|_{S_1} = -\frac{Q}{4\pi a^2}\sum_{l=0}^{\infty}\frac{(2l+1)\,h_l\,(kd)\,P_l(\cos\theta_1)}{kh_l'\,(ka)+i\sigma h_l\,(ka)}, \tag{7.5}$$

$$\left.\frac{\partial\psi}{\partial n}\right|_{S_1} = \frac{iQ\sigma_1}{4\pi a^2}\sum_{l=0}^{\infty}\frac{(2l+1)\,h_l\,(kd)\,P_l(\cos\theta_1)}{kh_l'\,(ka)+i\sigma h_l\,(ka)} = -i\sigma\;\psi|_{S_1}\,. \tag{7.6}$$

For the particular case of a sound-hard ($\sigma_1 = 0$) surfaces this gives

$$\psi|_{S_1} = -\frac{Q}{4\pi ka^2}\sum_{l=0}^{\infty}(2l+1)\,\frac{h_l\,(kd)}{h_l'\,(ka)}P_l(\cos\theta_1), \qquad \left.\frac{\partial\psi}{\partial n}\right|_{S_q} = 0, \tag{7.7}$$

while for sound-soft ($\sigma_1 = \infty$) surfaces we have

$$\psi|_{S_1} = 0, \qquad \left.\frac{\partial\psi}{\partial n}\right|_{S_1} = \frac{Q}{4\pi a^2}\sum_{l=0}^{\infty}(2l+1)\,\frac{h_l\,(kd)}{h_l\,(ka)}P_l(\cos\theta_1). \tag{7.8}$$

These formulae are classical and can be found elsewhere (e.g. see Hanish, 1981, pp.123-125).

7.1.2. Results of Computations. To test our software MultisphereHelmholtz for the case of a single sphere we compared results of computations of the potential on the surface with those provided by expression (7.7) and that obtained using the Boundary Element Method (BEM), as realized in the commercial software package COMET 4.0 from Collins and Aikman Automotive Interior Systems, Plymouth, MI. A typical output from this software package is shown in Fig. 7.1. The solution of the Helmholtz equation in a domain specified by a triangular surface mesh, and prescribed locations of the sources is shown.

The figures below illustrate comparisons of so-called "Head related transfer function" (HRTF) (see, e.g., Duda & Martens, 1998) computed using different methods. The HRTF is measured in dB and represents the ratio of the amplitude of the acoustic field at specified location of the surface to the amplitude of the incident field at the center of the sphere:

$$HRTF = 20\lg\left|\frac{\psi|_{S_1}}{\psi_{in}\,(\mathbf{r}_1')}\right|. \tag{7.9}$$

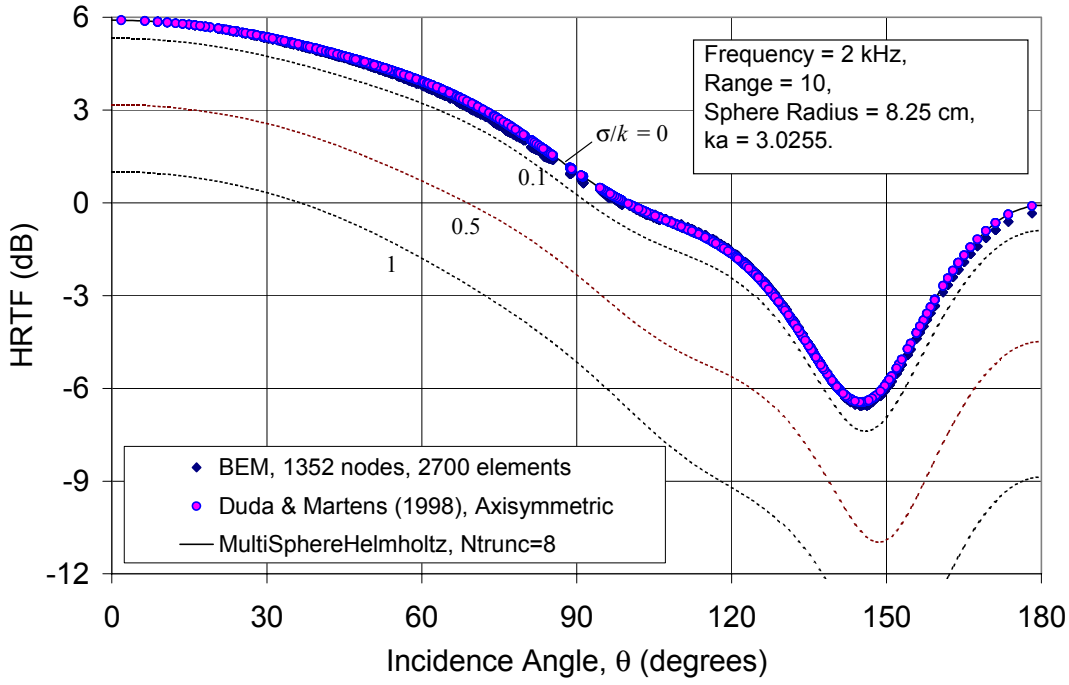

FIG. 7.2. *The head related transfer function (HRTF) for a single sphere of radius $a = 8.25$ cm and a monopole source, located at a distance $d/a = 10$ from the center of the sphere for spheres of different impedances σ/k (shown near curves). The continuous and dashed lines show results of computations using MultiSphereHelmholtz with truncation number $M = 8$. Circles and diamonds respectively show the results of Duda & Martens (1998) and of BEM computations for $\sigma = 0$. In the latter the sphere surface was discretized using 2700 linear elements.*

This function for a single sphere was investigated by Duda & Martens (1998), who used solution (7.7) for this purpose. They also provided a Matlab code for computations of the HRTF with truncation based on evaluation of the subsequent terms in the series (Duda, 2000).

Figure 7.2 shows good agreement between computations using all methods. In this example we include also computations for different impedances of the sphere.

We also tested the results of computations obtained using different truncation numbers. The original code of Duda & Martens (1998) uses truncation based on comparison of subsequent terms in the series (in this particular case the series was truncated when the ratio of such terms is smaller than 10^{-6}). Experiments with MultisphereHelmholtz showed that excellent agreement with these results is achieved, if the truncation number is selected using the formula (heuristic)

$$M = [eka]\,, \qquad e = 2.71828... \tag{7.10}$$

which shows that it increases with the wavenumber. For large ka good agreement was observed for $M \geqslant \left[\frac{1}{2}eka\right]$,while differences were visible for smaller M. For moderate ka such differences appeared for truncation numbers below the value provided in (7.10).

7.2. Two Spheres. Since there is no closed analytical solution for two spheres in a simple form, we compared numerical results obtained by using both our codes MultisphereHelmholtz and MultisphereHelmholtzCoaxial, and the BEM computations. As an example problem we considered computation of the HRTF for the so-called "Snowman model", used for simplified study of the generation of head pose related cues in an acoustic field.

The model consists of two spheres, which are touching at one point. In computations the ratio of sphere

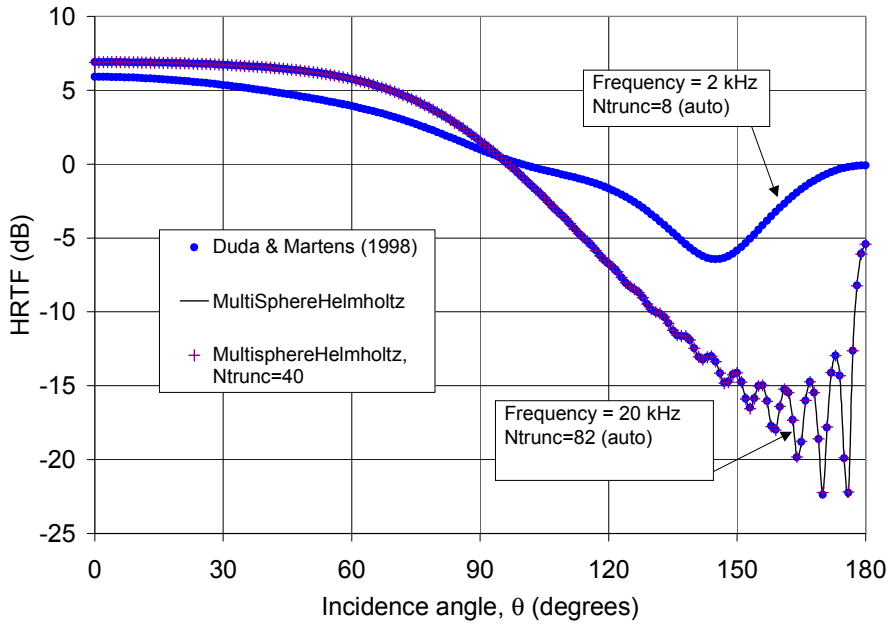

FIG. 7.3. *Computations of the HRTF for a sound-hard sphere ($\sigma = 0$) using the Duda & Martens (1998) solution with evaluation of the residual term in the series, and MultiSphereHelmholtz with automatic selection of the truncation number and $M = 40$ (for frequency 20 kHz). Other parameters are as in Fig 7.2.*

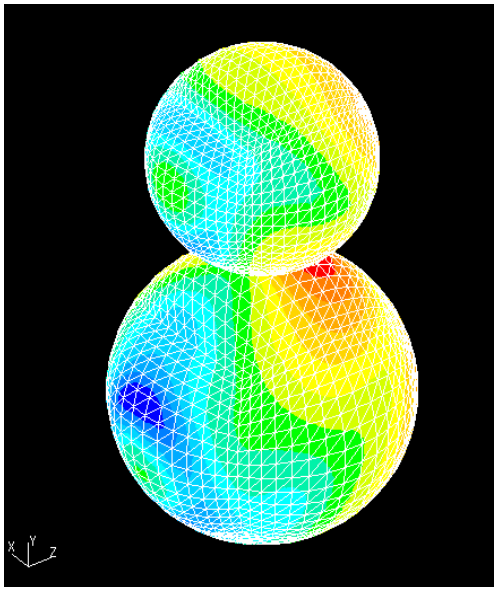

FIG. 7.4. *An example of BEM (COMET 4.0) computations of potential distribution over the surface of two spheres (Snowman model) generated by a monopole source. Each sphere surface is discretized to 2700 triangular elements. The ratio of sphere radii is 1.3253 and they touch in one point.*

radii was taken to be 1.3253. [2] The origin of the reference frame was located at the center of the smaller sphere (the "head") and the direction of the y-axis was from the larger sphere ("torso") to the head. The $z-$axis was directed towards a monopole source, generating the incident field, which was located at the

[2] Duda et al (2001) have performed measurements with a similar configuration. Comparison of simulations with these experiments will be reported shortly.

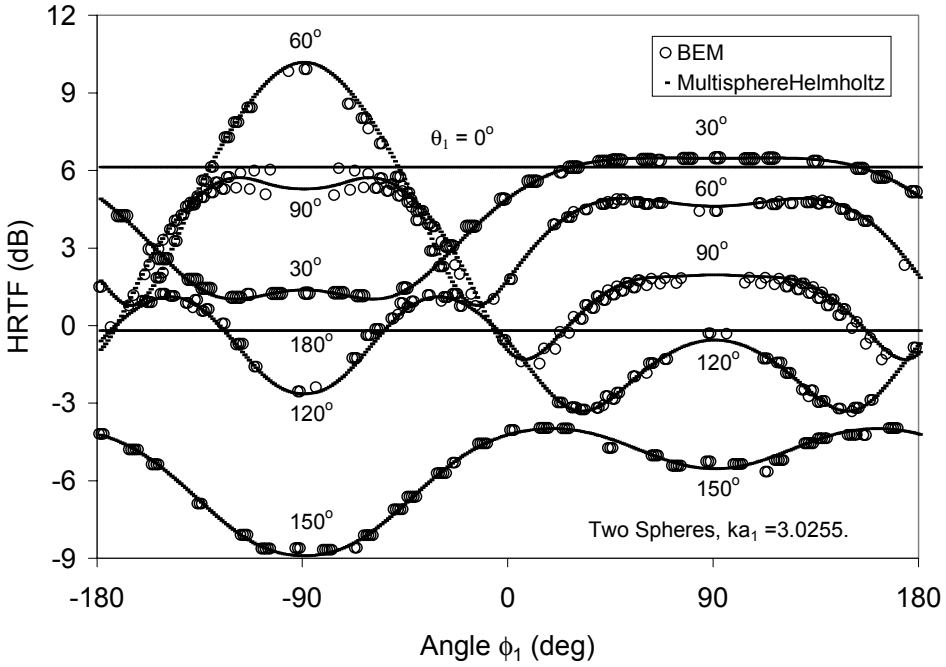

FIG. 7.5. *Comparison of the HRTF angular dependence over the surface of a smaller sphere computed for the two sphere geometry shown in Fig. 7.4 using the BEM and Multipole reexpansion technique (MultipoleHelmholtz). Both spheres have zero impedance.*

distance of 10 radii from the smaller sphere. The frequency of the incident wave nondimensionalized with the radius of the smaller sphere corresponded to $ka_1 = 3.0255$. The mesh for computations using BEM contained 5400 triangular elements (2700 elements for each sphere) and was obtained by mapping of the surface of the cube onto each sphere. A picture of this "Snowman" with computational mesh and distribution of the acoustic pressure is shown in Figure 7.4. In the computations the impedances of both spheres were set to zero ("sound-hard" surfaces).

For computations using MultisphereHelmholtz the truncation number was automatically set to

$$M = \left[\frac{1}{2}ekr'_{12}\right] \tag{7.11}$$

For given above values of a_2/a_1 and ka_1 this provided $M = 9$, so that the total number of modes n in the multipole expansion was 10 for each sphere (or 100 A_n^m coefficients for each sphere).

Figure 7.5 shows a comparison between the BEM and the MultisphereHelmholtz computational results for the HRTF calculated for sphere 1 according equation (7.9). Each curve corresponds to a fixed value of the spherical polar angle θ_1 and demonstrates dependence on the angle φ_1. Note that dependence on the angle φ_1 is only due to the presence of the sphere 2. Indeed in the absence of the torso, the potential distribution over the sphere 1 surface is axisymmetric (see the previous case of a single sphere), and there is no dependence on φ_1. The comparison shows a good agreement between the results obtained by different methods (the results produced by MultisphereHelmholtz and MultisphereHelmholtzCoaxial are on top of each other). Some small dispersion of the points obtained using BEM is due to the mesh discretization of the sphere surface, which normally can be avoided by additional smoothing/interpolation procedures. For the BEM results shown in the figure we did not apply such smoothing, but selected for plotting the values of potential at the element centers located within some small prescribed distance from a specified surface point (θ_1, φ_1). It is also noticeable that MultisphereHelmholtz far outperformed BEM computationally, both in much higher speed and memory usage.

Figure 7.6 demonstrate computations of the HRTF for the Snowman model with the parameters described above, but for higher frequency, and different impedances of the larger sphere (which can somehow model

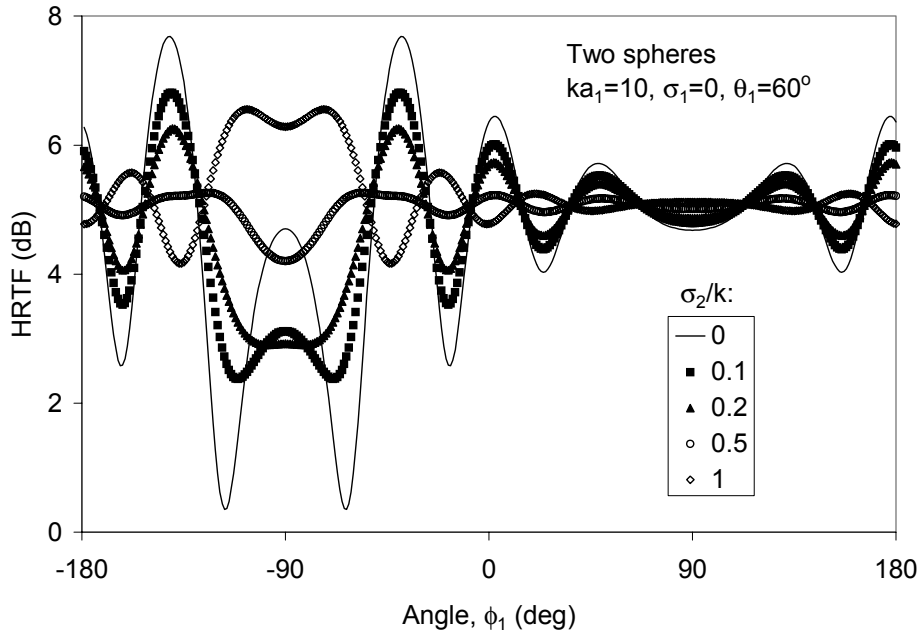

FIG. 7.6. *Angular dependence of the HRTF over the surface of the sound-hard smaller sphere for the geometry shown in Fig. 7.4 for different impedances of the larger sphere. Results computed using the MultisphereHelmholtz code with the automatically selected truncation number* $N_t = 31$.

the presence of clothes). For the given geometry parameters the automatically selected truncation number was $N_t = 31$. This number is large enough to observe a substantial difference in speed of computations and memory usage by MultisphereHelmholtz and MultisphereHelmholtzCoaxial (see evaluation (5.14), where $M = N_t$).

Proper selection of the truncation number is important issue for applications of multipole translation techniques. Figure 7.7 shows convergence of computations with increasing truncation numbers for the HRTF at any specified point on the surface ($\theta_1 = 60^\circ$ and $\varphi_1 = 0^\circ$ in the case shown in the figure). Computations with low truncation numbers may provide poor accuracy. At some truncation number (which depends on the frequency) the computational results stabilize (note that the HRTF depends on the frequency, and so for each frequency we have its own horizontal asymptote). Further increase of the truncation number increases both the accuracy of the results and computational time/memory, since the matrix size grows proportionally as N_t^4 in the general case, and as N_t^3 for coaxial spheres (so there is a trade-off issue). However, at some truncation numbers, which slightly exceed the value provided by (7.11), computations usually encounter difficulties connected with exponential growth of portions of the terms in the expansions, leading to overflow related errors. These are the spherical Hankel functions of large order, $h_n\left(kr'_{pq}\right)$, entering the reexpansion system matrix. Asymptotic expansion of the Hankel function at large n and fixed kr'_{12} shows, that the growth starts at $n \sim \frac{1}{2}ekr'_{12}$. This is used as the basis for automatic selection of the truncation number (7.11). Of course, this limitation is purely based on the order of computation, and the product of terms remain finite, and calculations can be performed for larger N_t than given by (7.11). To develop software using such sums of finite terms additional study of the truncated tails of the series at large n is needed, and a proper implementation remains to be developed.

The computations presented in Figure 7.7 show that the actual stabilization occurs at smaller N_ts than the one given by (7.11) (where we have for $ka_1 = 1, 5, 10, 20, 30$ the following values: $N_t = 3, 15, 31, 63, 94$, respectively. Results of our numerical experiments show that for large kr'_{12} reasonable accuracy can be achieved at $M^* \sim \frac{1}{2}M_{\max}$, where $M_{\max}$ is provided by equation (7.11). At the same time, for lower kr'_{12} formula (7.11) provides values which cannot be reduced, and accurate computations can be achieved with M slightly larger than $M_{\min}$, with $M_{\min}$ is provided by equation (7.11).

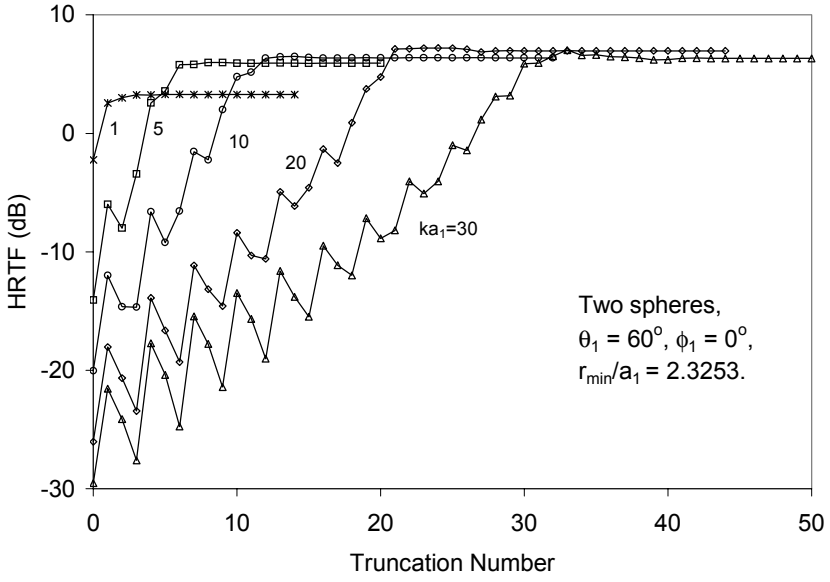

FIG. 7.7. *Dependences of compuations of the HRTF for two sphere geometry (see Fig. 7.4) on the multipole series truncation number for different non-dimensional wavenumbers.*

Note that in our previous paper (**GD2001**b) we also presented results of the computation of the HRTF for a sphere near a rigid wall. In this case the rigid wall could be replaced by an image sphere and an image source and the coaxial multipole reexpansion can be used. The problem of sound scattering by a sphere near a rigid wall is in some sense a simplified general problem for two spheres, since both the real and the image spheres in this case have the same radius and impedance. For this case, the coefficients of the multipole expansions near each sphere $A_n^{(1)m}$ and $A_n^{(2)m}$ are symmetrical and the dimension of the system can be reduced using this symmetry by a factor of two. In that paper, we also provided a study and discussion of the influence of the distance between the sphere and the wall and frequency of the field on the HRTF. Selected results of the HRTF for the Snowman model including comparisons with experimental data were also presented in Gumerov et al (2001).

7.3. Three Arbitrarily Located Spheres. If the cases of one and two spheres can be covered using simplified codes, the case of three non-coaxial spheres requires the general three-dimensional multipole translation developed in **GD2001**. As in the case of two spheres discussed above, we compared results of computations for three spheres using MultisphereHelmholtz and the COMET commercial BEM software.

For this computational example we placed an additional sphere (#3) to the case of the Snowman model, described above. The radius of the sphere was equal to the radius of the head, and it may model some object of the size of the head placed between the sound source and the listener. The distance between the centers of spheres #1 and #3 was the same as the distance between the centers of spheres #1 and #2. The parameters of the incident field were the same as.$for$the snowman case. The mesh for computations using the BEM contained 5184 triangular elements, 1728 elements for each sphere and was obtained by mapping of the surface of the cube to each sphere. A picture of this configuration with computational mesh and distribution of the acoustic pressure is shown in Figure 7.8. In computations the impedances of all three spheres were set to zero.

Results of comparisons between BEM and MultisphereHelmholtz computations with $M = 9$ are shown in Figure 7.9. The comparison is as good as in the case of two spheres. Since Figures 7.5 and 7.9 represent similar dependences, we can notice that the presence of the third sphere reduced (at some points by 3-4 dB) the amplitude of the sound field on sphere 1. This is a clear physical effect, since sphere 1 was situated in the acoustic shadow of sphere 3.

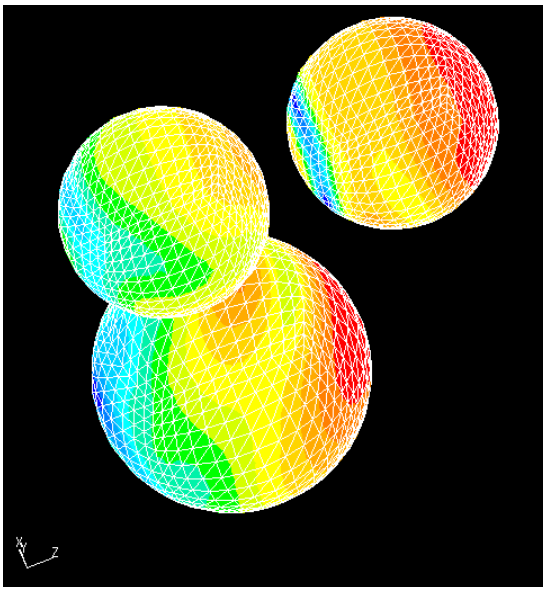

FIG. 7.8. *An example of BEM (COMET 4.0) computations of the potential distribution over the surface of three spheres generated by a monopole source. Each sphere surface is discretized to 1728 triangular elements. Two spheres of relative radii 1 (#1) and 1.3253 (#2) touch in one point and the ceneter of the third sphere (#3) of relative radius 1 is located at the distance 2.3253 from the center of sphere #1 on the line connected the source and the center of sphere #1.*

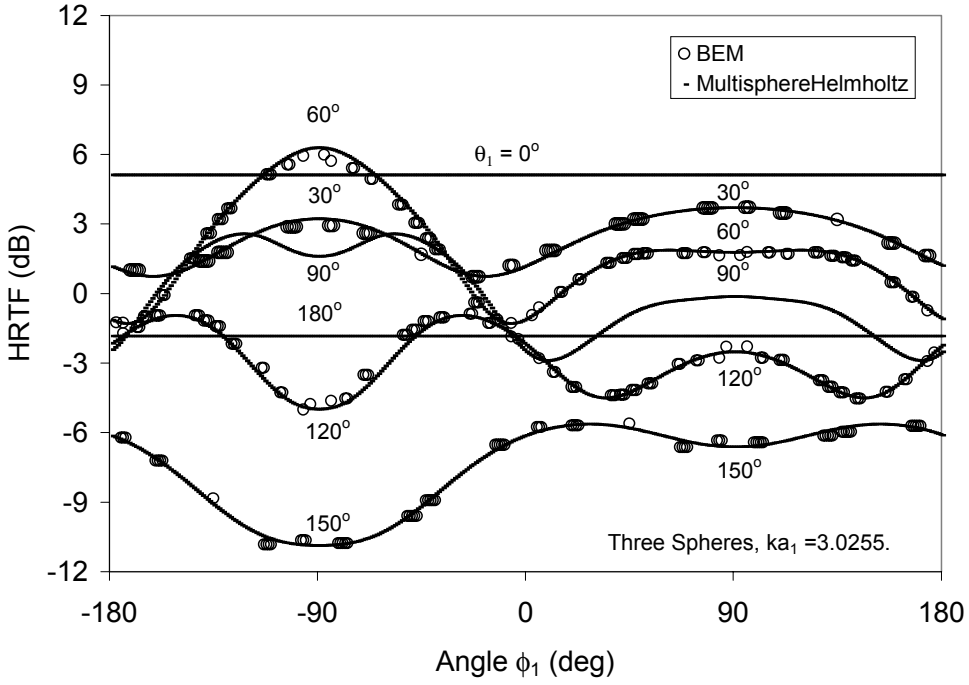

FIG. 7.9. *Comparison of the HRTF angular dependence over the surface of smaller sphere computed for the three sphere geometry shown in Fig. 7.4 using the BEM and Multipole reexpansion technique (MultipoleHelmholtz). All three spheres have zero impedance.*

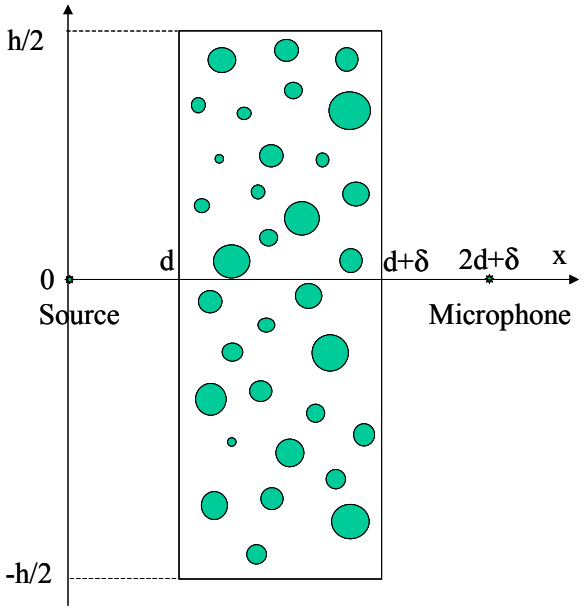

FIG. 7.10. *A sketch of the problem geometry for sound propagation through a screen of spherical particles.*

7.4. Many Spheres. The case of sound and electromagnetic wave scattering (both described by the Helmholtz equation) by many arbitrarily located spheres has numerous practical and theoretical applications, including acoustics and hydrodynamics of multiphase flows, sound propagation in composite materials, electromagnetic waves in clouds, and inverse problems, such as the detection of buried objects, medical tomography, etc. There is also a need to evaluate the acoustic scattering by multiple spheres in room acoustics, where the walls of the room are replaced by image spheres.

Let us consider the problem of sound scattering by a screen of spherical particles. The geometry of the problem is shown in Figure 7.10. Here the incident field is generated by a monopole source located at distance d from a flat particle screen of thickness δ. A microphone, measuring the acoustic pressure is located behind the screen at the same distance as the source. N spheres with the same acoustic impedance (in the examples below we set $\sigma = 0$), but with possibly different sizes are distributed according to some distribution density over their radii, and, have locations of their centers within a box $\delta \times h \times h$ representing the screen. The objective is to evaluate the effect of the screen on the sound propagation.

This effect can be evaluated using a "Screen Transfer Function" (STF), which we define as

$$STF = 20 \lg \left| \frac{\psi\left(\mathbf{r}'_{mic}\right)}{\psi_{in}\left(\mathbf{r}'_{mic}\right)} \right|, \tag{7.12}$$

where $\mathbf{r}'_{mic}$ is the radius-vector of the microphone location and which is measured in decibels.

Two examples of computations with many spheres are presented below. In the first example we placed 16 spheres with uniform random distribution of their dimensionless radii from $a_{\min} = 0.5$ to $a_{\max} = 1.5$. Dimensionless parameters of the screen were $d = 10$, $\delta = 5$, and $h = 50$. The sphere centers were distributed uniformly within the screen. The view of this screen in the yz-plane is shown in Figure 7.11. In computations we took three different wavenumbers, $ka = 1$, $ka = 3$, and $ka = 5$, where a is the length scale (the characteristic sphere radius). Computations were performed using MultisphereHelmholtz with increasing truncation number N_t. Dependences of the STF on N_t at various ka are and results are shown in Figure 7.12. It is seen that results converge to some value depending on ka. This type of check shows that for the given geometry relatively low truncation numbers can be used, which are much smaller than given by (7.11), where instead of r'_{12} some representative intersphere distance r'_{pq} is selected. We noticed however, that in some cases when we have many spheres with very different intersphere distances (from touching spheres, to spheres located at large kr'_{pq}), stabilization of computation only occurs at higher truncation numbers than prescribed by (7.11). Thus, at this point we can recommend to conduct several numerical experiments

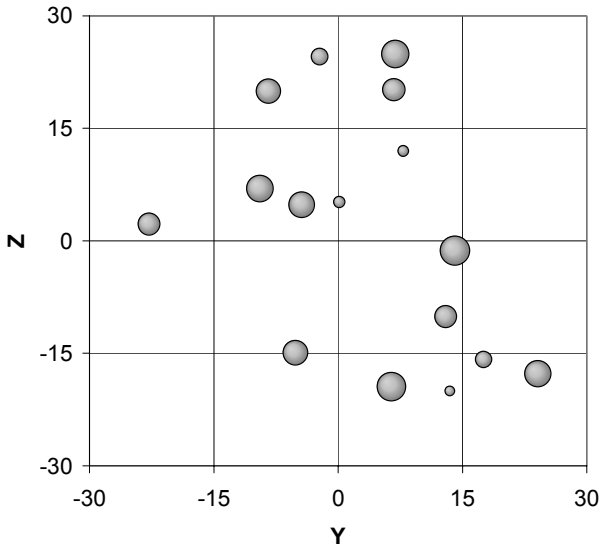

FIG. 7.11. *A scattering screen of 16 spheres of random size and random location of their centers. The centers are uniformly distributed inside a box* $10 < x < 15$, $-25 < y < 25$, $-25 < z < 25$. *The radii are uniformly distributed over* $0.5 < a < 1.5$.

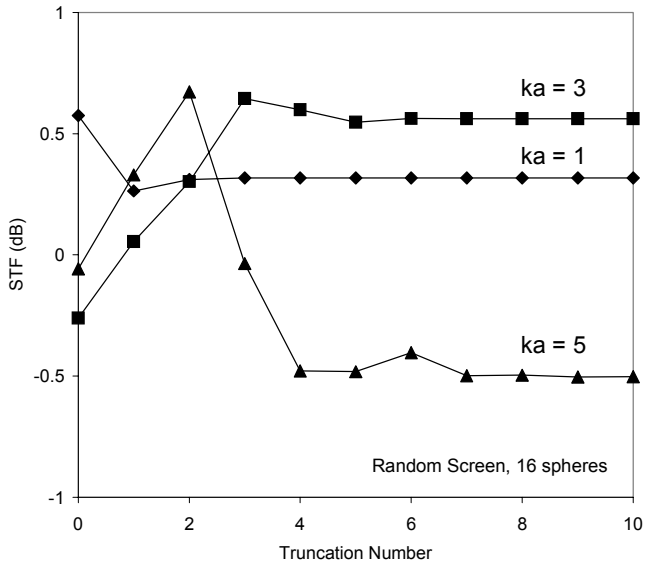

FIG. 7.12. *Convergence test for the problem of sound scattering by a screen of 16 randomly sized spheres with random location of their centers (as shown in Figure 7.11). Three different curves computed at different* ka,*where* a *is the mean of the sphere radii distribution.*

and check if the results are stable to variations in the truncation number to ensure its proper selection. A separate analytical study of the truncation number selection problem is required.

In the second example we put a regular monolayer screen ($d = 10$, $\delta = 0$, and $h = 50$) of 121 spheres of the same radii $a = 1$, which centers form a regular grid in plane $x = d$ (see Figure 7.13). Again we compared results obtained with the aid of MultisphereHelmholtz at increasing M and different wavenumbers and found fast convergence (see Figure 7.14).

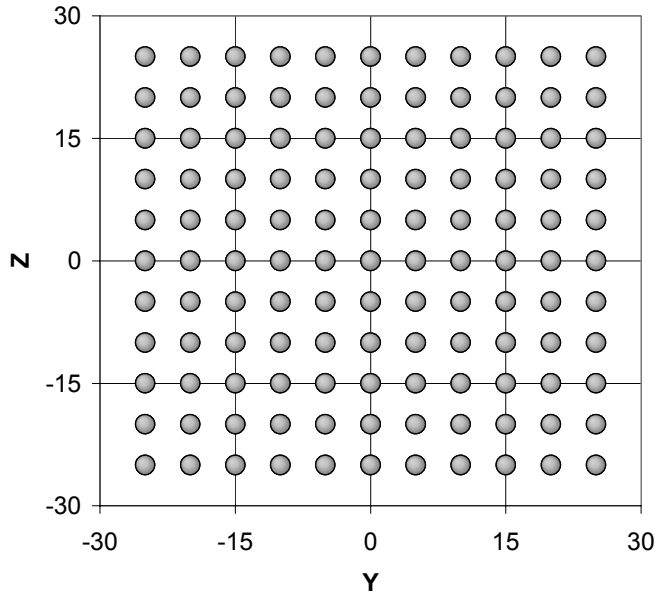

FIG. 7.13. *The view of a scattering screen of 121 spheres of the same size* $a = 1$ *and location of their centers at the nodes of a square grid* $-25 < y < 25$, $-25 < z < 25$ *with the grid size* $\Delta y = \Delta z = 5$.

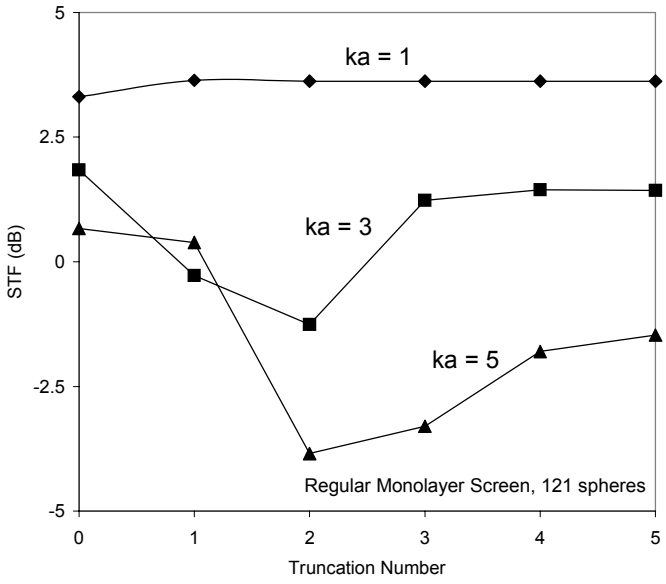

FIG. 7.14. *Convergence test for the problem of sound scattering by a screen of 121 equal sized spheres located at the nodes of a regular grid (as shown in Figure 7.13). Three different curves are computed at different* $\mathbf{ka}$ *indicated near the curves.*

8. Conclusions and Future Work. We have developed an analytical solution for sound, electromagnetic, or other wave propagation described by the Helmholtz equation for the case of N spheres of various radii and impedances arbitrary located in three dimensional space. This analytical solution uses a multipole reexpansion technique and involves infinite series and requires inversion of infinite matrices. We developed codes (MultisphereHelmholtz and MultisphereHelmholtzCoaxial) which are capable of computing the corresponding approximate solutions, based on these series and matrix truncations. These use the multipole reexpansion techniques described in our previous report (**GD2001**). We validated the codes by comparison

with previous analytical solutions for a single-sound hard sphere, with computational results for two and three spheres obtained using the Boundary Element Method with fine discretization of the surfaces (thousands of elements), and by convergence of the results obtained with different truncation numbers in the case of large numbers of spheres.

Concerning the performance of the codes we make the following conclusions:

- For good performance of the codes the truncation number, depending on the wavenumber, sphere sizes, and intersphere distances should be selected properly. In case the truncation mumber is properly selected, the codes showed high accuracy, and substantial speed-up in comparison to the Boundary Element Method.
- In cases when the centers of the spheres are located on a line (which is always true for two spheres, and can be realized in particular problems for N spheres) computations using a coaxial multipole reexpansion can be performed with higher efficiency, than in the general case. The CPU time and memory usage in the case of high truncation numbers (high frequencies or wave numbers) is much smaller using relations for coaxial multipole translation.

The objectives of the present study were to develop a solution for wave scattering by multiple spheres and to realize efficient computational algorithms for the problem, since we had a practical need for this solution. Based on our results, we propose the following as possibilities for future work:

- The present method takes into account all cross-influences between the spheres to equal degree. Efficient evaluation of the fields scattered by spheres remote from a considered object can be very useful and practical. This can enable reduction of the number of coefficients, the size of the linear system or make its properties convenient for efficient computation (e.g. make it sparse, block-structured, and so on). This also can enable reduction of truncation number, since it depends on the intersphere distances, and the influence of the remote objects happens through high harmonics that, generally speaking, requires unnecessary increase of the truncation numbers.
- Evaluate theoretically error bounds of truncation. Provide computationally efficient way for evaluation of truncated "tails" of the series of multipoles in the problem of N spheres.
- Consider application of "diagonalization" procedures, such as rotation-coaxial translation multipole reexpansion operators (**GD2001**), to the problem of N-spheres. This may lead to increase of computational efficiency in general case (in the present study we developed/implemented this method only for coaxial spheres).
- Analyze the present code MultisphereHelmholtz with a purpose to increase it efficiency using parallel computing. For example, since the system matrix consists of blocks, characterizing influence of one sphere to another, such block can be computed independently on the other blocks. For N spheres, up to $\frac{1}{2}N(N-1)$ parallel processes can be used to compute the system matrix. This also will lead efficiency in memory usage, since it will not require storage of harmonics for each pair of spheres.
- Due to the efficiency of solutions using multipole expansions consider modifications of the problem for N spheres for non-spherical objects to enable multipole reexpansion technique.

REFERENCES

[1] **N.A. Gumerov & R. Duraiswami (2001)** Fast, Exact, and Stable Computation of Multipole Translation and Rotation Coefficients for the 3-D Helmholtz Equation. Institute for Advanced Computer Studies Technical Report UMIACS-TR-# 2001-44, Also issued as Computer Science Technical Report CS-TR-# 4264.

[2] **M.A. Epton and B. Dembart (1995)** Multipole translation theory for the three-dimensional Laplace and Helmholtz equations, *SIAM J. Scientific Computing*, 4 (16), pp. 865-897.

[3] **S. Koc, J. Song & W.C. Chew (1999)** Error analysis for the numerical evaluation of the diagonal forms of the scalar spherical addition theorem, *SIAM J. Numer. Anal.*, 36(3), pp. 906-921.

[4] **N.A. Gumerov & R. Duraiswami (2001b)** Modeling the effect of a nearby boundary on the HRTF. International Conference on Acoustics, Speech, and Signal Processing 2001, Salt Lake City, Utah, May 7-11, 2001.

[5] **N.A. Gumerov, Z. Tang, R. Duraiswami, R.O. Duda, V.R. Algazi & S. T. Raveendra (2001c)** Modeling the effect of torso on the head-related transfer function via the boundary element method. The 141st Meeting of the of the Acoustical Society of America (ASA) Chicago, Illinois, USA, June 4-8.

[6] **P.M. Morse and H. Feshbach**, *Methods of Theoretical Physics -I*, McGraw-Hill, 1953.

[7] **M. Abramowitz and I.A. Stegun**. *Handbook of Mathematical Functions*, National Bureau of Standards, Wash., D.C.,1964.

[8] **Richard O. Duda** (personal communication). Matlab software for computing spherical HRTFs.

[9] **S. Hanish,** A Treatise on Acoustic Radiation, Naval Research Laboratory, Washington, D.C., 1981.

[10] **R.O. Duda & W.L. Martens,** Range dependence of the response of a spherical head model, J. Acoust. Soc. Am. 104, 1998, 3048-3058.
[11] **J. W. Strutt (Lord Rayleigh).** On the acoustic shadow of a sphere, Philos. Trans. R. Soc. London, Ser. A 203, 8789, 1904.
[12] **J.W. Strutt (Lord Rayleigh).** The Theory of Sound, Dover, New York, 2nd ed., Vols. 1 and 2., 1945.
[13] **R.O.Duda, V.Ralph Algazi, Dennis Thompson**, (personal communication), "Results of Snowman Tests"
[14] **Ramani Duraiswami, Nail A. Gumerov, Larry Davis, Shihab A. Shamma, and Howard C. Elman, Richard O. Duda and V. Ralph Algazi, Qing-Huo Liu, S. T. Raveendra**, "Individualized HRTFs using computer vision and computational acoustics," J. Acoust. Soc. Am., 108, p. 2597, 2000.
[15] **R. Duraiswami and A. Prosperetti**. "Linear Pressure Waves in Fogs," J. Fluid Mech., vol. 299, pp. 187-215, 1995.
[16] **N.A. Gumerov, A.I. Ivandaev & R.I. Nigmatulin.** "Sound waves in monodisperse gas-particle or vapour-droplet mixtures." J. Fluid Mech., 193, 53-74, 1988.
[17] **Ramani Duraiswami, Nail A. Gumerov, Dmitry N. Zotkin, Larry S. Davis**, "Efficient Evaluation of Reverberant Sound Fields," accepted for presentation at the 2001 IEEE Workshop on Applications of Signal Processing to Audio and Acoustics, Mohonk Mountain Hose, New Palz, NY.